

# Importance of Magnetic Helicity in Dynamos

Axel Brandenburg

Nordita, Blegdamsvej 17, 2100 Copenhagen Ø, Denmark  
brandenb@nordita.dk

Magnetic helicity is nearly conserved and its evolution equation provides a dynamical feedback on the alpha effect that is distinct from the conventional algebraic alpha quenching. The seriousness of this dynamical alpha quenching is particularly evident in the case of closed or periodic boxes. The explicit connection with catastrophic alpha quenching is reviewed and the alleviating effects of magnetic and current helicity fluxes are discussed.

## 1 Introduction

Let us begin by defining dynamos and helicity. Dynamos are a class of velocity fields that allow a weak seed magnetic field to be amplified until some saturation process sets in. Mathematically, this is described by exponentially growing solutions of the induction equation. Simulations have shown that any sufficiently complex flow field can act as a dynamo if the resistivity is below a certain threshold. It is in principle not even necessary that the flow is three-dimensional, only the magnetic field must be three-dimensional because otherwise one of several antidynamo theorems apply (Cowling, 1934; Zeldovich, 1957).

Helicity, on the other hand, quantifies the swirl in a vector field. There is kinetic helicity, which describes the degree to which vortex lines follow a screw-like pattern, and it is positive for right-handed screws. Examples of helical flows are the highs and lows on the weather map. For both highs and lows the kinetic helicity has the same sign and is negative (positive) in the northern (southern) hemisphere. For example, in an atmospheric low, air flows inward, i.e. toward the core of the vortex, and down to the bottom of the atmosphere, but the Coriolis force makes it spin anti-clockwise, causing left-handed spiraling motions and hence negative helicity.

A connection between helicity and dynamos has been established already quite some time ago when Steenbeck et al. (1966) calculated the now famous  $\alpha$  effect in mean field dynamo theory and explained its connection with kinetic helicity. In this paper we are not so much concerned with kinetic helicity, but mostly with the magnetic and current helicities. Quantifying the swirl of magnetic field lines has diagnostic significance, because magnetic helicity is a topological invariant of the ideal (non-resistive) equations. Especially in the solar community the *diagnostic* properties of magnetic helicity have been exploited extensively over the past decade. However, the use of magnetic helicity as a *prognostic* quantity for understanding the governing nonlinearity of  $\alpha$  effect dynamos has only recently been noted in connection with the magnetic helicity constraint (Brandenburg, 2001, hereafter referred to as B01).

We should emphasize from the beginning that dynamos do not have to have helicity. The small-scale dynamo of [Kazantsev \(1968\)](#) is an example of a dynamo that works even without helicity. Nonhelical dynamos are generally harder to excite than helical dynamos, but both can generate fields of appreciable strength if the magnetic Reynolds number is large. The stretch-twist-fold dynamo also operates with twist (as the name suggests!), but the orientation of twist can be random, so the net helicity can be zero. Simulations have shown that even with zero helicity density everywhere, dynamos can work ([Hughes et al., 1996](#)).

It is also possible to generate magnetic fields of large scale once there is strong shear, even if there is no helicity ([Vishniac and Brandenburg, 1997](#)). This case is very much a topic of current research. One of the possibilities is the so-called shear-current effect ([Rogachevskii and Kleeorin, 2003, 2004](#)), but such dynamos still produce helical large-scale magnetic fields. There is also the possibility of an intrinsically nonlinear dynamo operating with magnetic helicity flux alone ([Vishniac and Cho, 2001](#)). Thus, it is not necessarily clear that large-scale dynamos have to work with kinetic helicity and the corresponding  $\alpha$  effect. However, there is as yet no convincing example of a dynamo without the involvement of kinetic helicity that generates large-scale magnetic fields with a degree of coherence that is similar to that observed in stars and in galaxies, e.g. cyclically migrating magnetic fields in the sun and grand magnetic spirals in some nearby galaxies. Such fields can potentially be generated by dynamos with an  $\alpha$  effect, as has been shown in many papers over the past 40 years; see Chaps. 2, 4, and 6.

There is however a major problem with  $\alpha$  effect dynamos; see [Brandenburg \(2003\)](#); [Brandenburg and Subramanian \(2005\)](#) for recent reviews on the issue. The degree of severity depends on the nature of the problem. It is most severe in the case of a homogeneous  $\alpha$  effect in a periodic box, which is also when the problem shows up most pronouncedly. [Cattaneo and Hughes \(1996\)](#) found that the  $\alpha$  effect is quenched to resistively small values once the mean field becomes a fraction of the equipartition field strength. In response to such difficulties three different approaches have been pursued. The most practical one is to simply ignore the problem and proceed as if we can still use the  $\alpha$  effect with a quenching that only sets in at equipartition field strengths. This can partially be justified by the apparent success in applying this theory; see the recent reviews by [Beck et al. \(1996\)](#); [Kulsrud \(1999\)](#), and [Widrow \(2002\)](#). The second approach is to resort to direct three dimensional simulations of the turbulence in such astrophysical bodies. In the solar community this approach has been pioneered by [Gilman \(1983\)](#) and [Glatzmaier \(1985\)](#), and more recently by [Brun et al. \(2004\)](#). The third approach is a combination of the first two, i.e. to use direct simulations of problems where mean-field theory should give a definitive answer. This is also the approach taken in the present work. The hope is ultimately to find guidance toward a revised mean-field theory and to test it quantitatively. A lot of progress has already been made which led to the suggestion that only a dynamical (i.e. explicitly time dependent) theory of  $\alpha$  quenching is compatible with the simulation results. In the present paper we review some of the simulations that have led to this revised understanding of mean-field theory.

The dynamical quenching theory is now quite successful in reproducing the results from simulations in a closed or periodic box with and without shear. In these cases super-equipartition fields are possible, but only after a resistively long

time scale. In the case of an open box without shear the dynamical quenching theory is also successful in reproducing the results of simulations, but here the root mean-field strength decreases with increasing magnetic Reynolds number, suggesting that such a dynamo is unimportant for astrophysical applications. Open boxes with shear appear now quite promising, but the theory is still incomplete and, not surprisingly, there are discrepancies between simulations and theory. In fact, it is quite possible that it is not even the  $\alpha$  effect that is important for large-scale field regeneration. Alternatives include the shear-current effect of Rogachevskii and Kleeorin (2003, 2004) and the Vishniac and Cho (2001) magnetic and current helicity fluxes. In both cases strong helicity fluxes are predicted by the theory and such fluxes are certainly also confirmed observationally for the sun (Berger and Ruzmaikin, 2000; DeVore, 2000; Chae, 2000; Low, 2001). For the galaxy the issue of magnetic helicity is still very much in its infancy, but some first attempts in this direction are already being discussed (Shukurov, 2005).

## 2 Dynamos in a Periodic Box

To avoid the impression that all dynamos have to have helicity, we begin by commenting explicitly on dynamos that do not have net kinetic helicity, i.e.  $|\langle \boldsymbol{\omega} \cdot \mathbf{u} \rangle| / (k_f \langle \mathbf{u}^2 \rangle) \ll 1$ , where  $k_f$  is the wavenumber of the forcing (corresponding to the energy carrying scale). Unless the flow also possesses some large-scale shear flow (discussed separately in Sect. 4.5 below), such dynamos are referred to as small-scale dynamos. The statement made in the introduction that *any* sufficiently complex flow field can act as a dynamo is really only based on experience, and the statement may need to be qualified for small-scale dynamos. Indeed, whether or not turbulent small-scale dynamos work in stars where the magnetic Prandtl numbers are small ( $\text{Pr}_M \approx 10^{-4}$ ) is unclear (Schekochihin et al., 2004; Boldyrev and Cattaneo, 2004). Simulations suggest that the critical magnetic Reynolds numbers increase with decreasing magnetic Prandtl number like  $R_{m,\text{crit}} \approx 35\text{Pr}_M$  (Haugen et al., 2004).

Throughout the rest of this review, we want to focus attention on large scale dynamos. This is where magnetic helicity plays an important role. Before we explain why in a periodic box nonlinear dynamos operate only on a resistively slow time scale, it may be useful to illustrate the problem with some numerical facts.

In the simulations of B01 the flow was forced at an intermediate wavenumber,  $k \approx k_f = 5$ , while the smallest wavenumber in the computational domain corresponds to  $k = k_1 = 1$ . The kinetic energy spectrum peaks at  $k \approx k_f$ , which is therefore also the wavenumber of the energy carrying scale. The turbulence is nearly fully helical with  $\langle \boldsymbol{\omega} \cdot \mathbf{u} \rangle / (k_f \langle \mathbf{u}^2 \rangle) \approx 0.7 \dots 0.9$ . The initial field is random, but as time goes on it develops a large-scale component at wavenumber  $k \approx k_1 = 1$ ; see Fig. 1. In Fig. 2 we show the evolution of the magnetic energy of the mean field from the same simulation.<sup>1</sup> Here the mean field is defined as two-dimensional averages over planes perpendicular to the direction in which the mean field varies. There are of course three such directions, but there is usually only one direction for which there is a significant mean field.

<sup>1</sup> Here the time unit is  $[t] = (c_s k_1)^{-1}$ , where  $c_s$  is the isothermal speed of sound, and the magnetic field is measured in units of  $[B] = \sqrt{\mu_0 \rho_0} c_s$ .

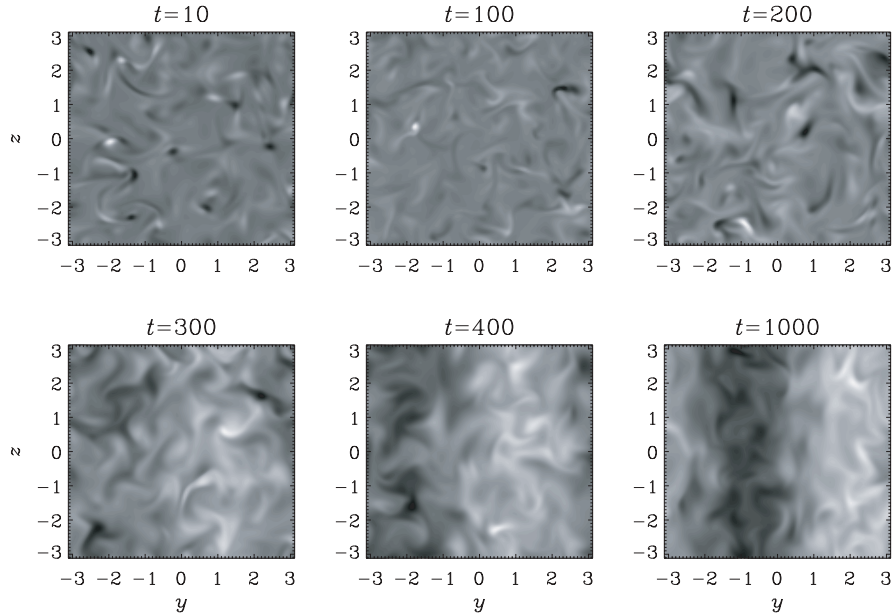


**Fig. 1.** Cross-sections of  $B_x(0, y, z)$  for Run 3 of B01 at different times showing the gradual build-up of the large-scale magnetic field after  $t = 300$ . The diffusive time scale for this run is  $(\eta k_1^2)^{-1} = 500$ . Dark (light) corresponds to negative (positive) values. Each image is scaled with respect to its min and max values. The final state corresponds to the second eigenfunction given in (33), but with some smaller scale turbulence superimposed [Adapted from Brandenburg and Subramanian (2005)]

While the saturation field strength increases with increasing magnetic Reynolds number, the time scale on which this nonlinear dynamo saturates increases too. To avoid misunderstandings, it is important to emphasize that this result applies only when we are in the *nonlinear regime* and when the flows are *helical*.

In turbulence one is used to situations where the microscopic values of viscosity  $\nu$  and magnetic diffusivity  $\eta$  do not matter in the sense that, for almost all practical purposes, they are superseded by turbulent effective values,  $\nu_t$  and  $\eta_t$ , respectively. This is because in turbulence there is spectral energy all the way down to the viscous/resistive length scale,  $(\eta\tau)^{1/2}$ , where  $\tau$  is the turnover time.<sup>2</sup> Thus, even when  $\nu$  is very small, the rate of viscous dissipation,  $\langle 2\nu\rho\mathbf{S}^2 \rangle$ , is in general finite ( $\mathbf{S}$  is the trace-less rate of strain tensor). Likewise, even when  $\eta$  is very small, the rate of Joule dissipation,  $\eta\mu_0\langle \mathbf{J}^2 \rangle$ , is in general finite ( $\mu_0$  is the magnetic permeability). This is because the current density diverges with decreasing  $\eta$  like  $|\mathbf{J}| \sim \eta^{-1/2}$ , so the energy dissipation stays finite and asymptotically independent of how small  $\eta$  is. The trouble is that the value of magnetic helicity dissipation is proportional

<sup>2</sup> The turnover time at the wavenumber  $k$  is  $(u_k k)^{-1}$ . Using Kolmogorov scaling,  $u_k \sim k^{-1/3}$ , one finds the familiar formula  $k_\eta = k_f R_m^{3/4}$ , where  $k_f$  is the wavenumber of the energy carrying eddies.

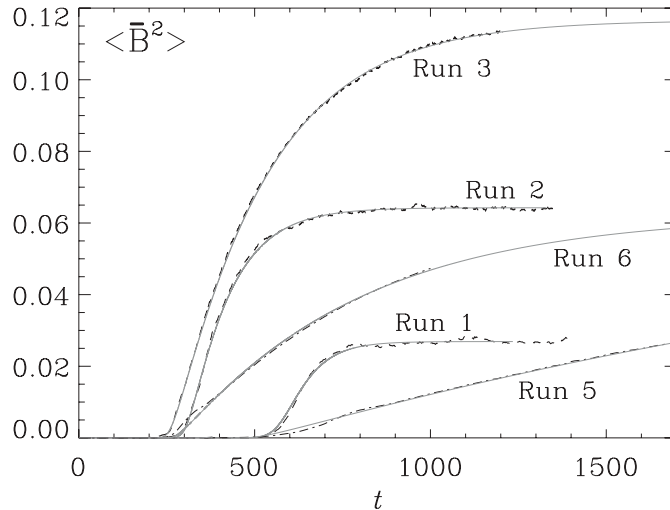


**Fig. 2.** Evolution of  $\langle \bar{B}^2 \rangle$  for Runs 1–3 and 5, 6 (*dashed lines*). The magnetic Reynolds numbers are  $R_m \equiv u_{\text{rms}}/\eta k_f = 2.4, 6, 18, 100,$  and  $16,$  respectively; see B01. The *solid lines* denote the solution of the associated mean-field dynamo problem where *both*  $\alpha$  and turbulent diffusivity  $\eta_t$  are quenched in a magnetic Reynolds number dependent fashion [Adapted from B01]

to  $\eta \langle \mathbf{J} \cdot \mathbf{B} \rangle$  (see below), and in the limit  $\eta \rightarrow 0$  we have  $\eta \langle \mathbf{J} \cdot \mathbf{B} \rangle \rightarrow \eta^{1/2} \rightarrow 0$ , so resistive magnetic helicity dissipation becomes impossible in the limit of large  $R_m$ . In the following section we derive and discuss the evolution equation for magnetic helicity.

### 3 Magnetic Helicity Evolution

#### 3.1 The Two-scale Property of Helical Turbulence

Usually in mean-field dynamo theory one talks about the two-scale *assumption* made in order to derive the mean-field equations (e.g. Moffatt, 1978; Krause and Rädler, 1980). This has to do with the fact that higher order derivatives in the mean field equation can only be neglected when the mean field is sufficiently smooth. Here, instead, we use the two-scale *properties* of helical turbulence as demonstrated in the previous section. These properties emerge automatically when the size of the whole body is at least several times larger than the scale of the turbulent eddies. As Fig. 1 shows explicitly, a large-scale field (wavenumber  $k_1$ ) emerges in addition to the forcing scale (wavenumber  $k_f \gg k_1$ ).

In this section we discuss the magnetic helicity equation and use it together with the two-scale property of helical turbulence to derive the so-called magnetic helicity constraint that allows the result of Fig. 2 to be understood quantitatively.

### 3.2 Definition of Helicity

The helicity of any solenoidal vector field  $\mathbf{f}$ , i.e. with  $\nabla \cdot \mathbf{f} = 0$ , is defined as the volume integral of  $\mathbf{f}$  dotted with its inverse curl, i.e.  $\text{curl}^{-1} \mathbf{f} \equiv \mathbf{g}$ . As pointed out by Moffatt (1969), the helicity quantifies the topological linkage between tubes in which  $\mathbf{f}$  is non-vanishing. In the following the linkage aspect of helicity will not be utilized, but rather the mathematical evolution equation that the helicity obeys (see the next section). However, the calculation of  $\mathbf{g}$  is problematic because it involves a gauge ambiguity in that the curl of  $\mathbf{g}' = \mathbf{g} + \nabla\phi$  also gives the same  $\mathbf{f} = \text{curl} \mathbf{g}'$ .

In the special case of periodic boundary conditions or for  $\hat{\mathbf{n}} \cdot \mathbf{f} = 0$  on the boundaries, where  $\hat{\mathbf{n}}$  is the normal vector on the boundary, the helicity is actually gauge-invariant, because

$$\begin{aligned} \int \mathbf{f} \cdot \mathbf{g}' \, dV &= \int \mathbf{f} \cdot \mathbf{g} \, dV + \int \mathbf{f} \cdot \nabla\phi \, dV \\ &= \int \mathbf{f} \cdot \mathbf{g} \, dV - \int \phi \nabla \cdot \mathbf{f} \, dV = \int \mathbf{f} \cdot \mathbf{g} \, dV, \end{aligned} \quad (1)$$

where we have used  $\nabla \cdot \mathbf{f} = 0$ . Since the magnetic field is divergence free, the magnetic helicity,  $\int \mathbf{B} \cdot \text{curl}^{-1} \mathbf{B} \, dV$  is gauge invariant. For other boundary conditions this is unfortunately not the case.

For vector fields whose inverse curl is a physically meaningful quantity, such as the vorticity  $\boldsymbol{\omega}$ , whose inverse curl is the velocity  $\mathbf{u}$ , the gauge question never arises. In this and similar cases the helicity density,  $\boldsymbol{\omega} \cdot \mathbf{u}$  in this case, is physically meaningful. Other examples are the cross helicity,  $\int \mathbf{B} \cdot \text{curl}^{-1} \boldsymbol{\omega} \, dV$ , which describes the linkage between magnetic flux tubes and vortex tubes, and the current helicity,  $\int \mathbf{J} \cdot \text{curl}^{-1} \mathbf{J} \, dV$ , which quantifies the linkage of current tubes. In these two cases it is natural to use  $\text{curl}^{-1} \mathbf{B} = \mathbf{A}$  and  $\text{curl}^{-1} \boldsymbol{\omega} = \mathbf{u}$ . For the magnetic field one can define the magnetic vector potential,  $\text{curl}^{-1} \mathbf{B} = \mathbf{A}$ , but  $\mathbf{A}$  is not a physically meaningful quantity and hence the magnetic helicity,

$$H = \int_V \mathbf{A} \cdot \mathbf{B} \, dV \equiv \langle \mathbf{A} \cdot \mathbf{B} \rangle V \quad (2)$$

is gauge-dependent, unless the boundaries of the volume  $V$  are periodic or perfectly conducting. Here and below, angular brackets denote volume averages. Occasionally, however, we simply refer to  $\langle \mathbf{A} \cdot \mathbf{B} \rangle$  as the magnetic helicity, but this is strictly speaking only the magnetic helicity per unit volume.

In the following section we derive the evolution equation for  $\langle \mathbf{A} \cdot \mathbf{B} \rangle$  and focus first on the case where the boundary conditions are indeed periodic, so  $\langle \mathbf{A} \cdot \mathbf{B} \rangle$  is gauge-invariant.

### 3.3 Derivation of the Magnetic Helicity Equation

The homogeneous Maxwell equations are

$$\frac{\partial \mathbf{B}}{\partial t} = -\nabla \times \mathbf{E}, \quad \nabla \cdot \mathbf{B} = 0. \quad (3)$$

Expressing this in terms of the magnetic vector potential,  $\mathbf{A}$ , where  $\mathbf{B} = \nabla \times \mathbf{A}$ , we have

$$\frac{\partial \mathbf{A}}{\partial t} = -\mathbf{E} - \nabla \phi, \quad (4)$$

where  $\phi$  is the scalar potential. Dotting (3) and (4) with  $\mathbf{A}$  and  $\mathbf{B}$ , respectively, and adding them, we have

$$\frac{\partial}{\partial t} \langle \mathbf{A} \cdot \mathbf{B} \rangle = -2\mathbf{E} \cdot \mathbf{B} - \nabla \cdot (\mathbf{E} \times \mathbf{A} + \phi \mathbf{B}). \quad (5)$$

Here,  $\mathbf{A} \cdot \mathbf{B}$  is the magnetic helicity density, but since it is not gauge invariant (see below) it is not a physically meaningful quantity. After integrating (5) over a periodic volume, the divergence term does not contribute. Furthermore, using Ohm's law,  $\mathbf{E} = -\mathbf{U} \times \mathbf{B} + \eta \mu_0 \mathbf{J}$ , where  $\mathbf{J} = \nabla \times \mathbf{B} / \mu_0$  is the current density, we have

$$\frac{d}{dt} \langle \mathbf{A} \cdot \mathbf{B} \rangle = -2\eta \mu_0 \langle \mathbf{J} \cdot \mathbf{B} \rangle, \quad (6)$$

i.e. the magnetic helicity,  $\langle \mathbf{A} \cdot \mathbf{B} \rangle$ , changes only at a rate that is proportional to  $\eta \langle \mathbf{J} \cdot \mathbf{B} \rangle$ . (Here and elsewhere, angular brackets denote volume averaging.) As discussed in the previous section, this rate converges to zero in the large  $R_m$  limit. Here, angular brackets denote volume averages, i.e.  $\langle \mathbf{A} \cdot \mathbf{B} \rangle = \frac{1}{V} \int_V \mathbf{A} \cdot \mathbf{B} dV$ .

We recall that for periodic boundary conditions,  $\langle \mathbf{A} \cdot \mathbf{B} \rangle$  is invariant under the transformation  $\mathbf{A} \rightarrow \mathbf{A}' = \mathbf{A} + \nabla \Lambda$ , which does not change the value of  $\mathbf{B}' = \nabla \times \mathbf{A}' = \nabla \times \mathbf{A} = \mathbf{B}$ . Here,  $\Lambda$  is a gauge potential. Thus, for periodic boundary conditions,  $\langle \mathbf{A} \cdot \mathbf{B} \rangle$  is a physically meaningful quantity. The same is also true for perfectly conducting boundaries (see [Brandenburg and Dobler, 2002](#), for corresponding simulations). For open boundaries, however,  $\int_V \mathbf{A} \cdot \mathbf{B} dV$  is not gauge invariant, but one can derive a gauge-invariant relative magnetic helicity ([Berger and Field, 1984](#)).

### 3.4 The Magnetic Helicity Constraint

A very simple argument can be made to explain the saturation level and the resistively slow saturation behavior observed in Fig. 2. The only assumption is that the turbulence is helical, i.e.  $\langle \boldsymbol{\omega} \cdot \mathbf{u} \rangle \neq 0$ , where  $\boldsymbol{\omega}$  is the vorticity, and that this introduces current helicity  $\langle \mathbf{j} \cdot \mathbf{b} \rangle$ , at the same scale and of the same sign as the kinetic helicity. Here we have split the field into large and small-scale fields, i.e.  $\mathbf{B} = \overline{\mathbf{B}} + \mathbf{b}$  and hence also  $\mathbf{J} = \overline{\mathbf{J}} + \mathbf{j}$  and  $\mathbf{A} = \overline{\mathbf{A}} + \mathbf{a}$ .

The first remarkable thing to note is that, even though we are dealing with *helical* dynamos, there is no net current helicity in the steady state, i.e.

$$\langle \mathbf{J} \cdot \mathbf{B} \rangle = 0; \quad (7)$$

see (6). However, using the decomposition into large and small-scale fields, we can write

$$\langle \mathbf{J} \cdot \mathbf{B} \rangle = \langle \overline{\mathbf{J}} \cdot \overline{\mathbf{B}} \rangle + \langle \mathbf{j} \cdot \mathbf{b} \rangle = 0, \quad (8)$$

so we have

$$\langle \overline{\mathbf{J}} \cdot \overline{\mathbf{B}} \rangle = -\langle \mathbf{j} \cdot \mathbf{b} \rangle \quad (9)$$

in the steady state. We now introduce the approximations<sup>3</sup>

<sup>3</sup> Here and elsewhere we use units where  $\mu_0 = 1$  or, following R. Blandford (private communication), we use units in which pi is one quarter.

$$\langle \bar{\mathbf{J}} \cdot \bar{\mathbf{B}} \rangle \approx k_m \langle \bar{\mathbf{B}}^2 \rangle \quad \text{and} \quad \langle \mathbf{j} \cdot \mathbf{b} \rangle \approx -k_f \langle \mathbf{b}^2 \rangle \quad (10)$$

where  $k_m$  and  $k_f$  are the typical wavenumbers of the mean and fluctuating fields, respectively. These approximations are only valid for fully helical turbulence, but can easily be generalized to the case of fractional helicity; see Sect. 4.1 and Blackman and Brandenburg (2002, hereafter BB02). We have furthermore assumed that the sign of the kinetic helicity is negative, as is the case in the northern hemisphere of the sun, for example. (The case of positive kinetic helicity is straightforward; see below.) The wavenumber  $k_f$  of the fluctuating field is for all practical purposes equal to the wavenumber of the forcing function. (In more general situations, such as convection or shear flow turbulence,  $k_f$  would be the wavenumber of the energy carrying eddies.) We also note that for large values of the magnetic Reynolds number,  $R_m$ , the  $k_f$  factor in (10) gets attenuated by an  $R_m^{1/4}$  factor (BB02). On the other hand, the wavenumber of the mean field is in practice the wavenumber of the box, i.e.  $k_m = k_1$ . Inserting now (10) into (9) yields

$$\langle \bar{\mathbf{B}}^2 \rangle = \frac{k_f}{k_m} \langle \mathbf{b}^2 \rangle, \quad (11)$$

i.e. the energy of the mean field can *exceed* the energy of the fluctuating field – in contrast to earlier expectations (e.g. (Vainshtein and Cattaneo, 1992; Kulsrud and Anderson, 1992; Gruzinov and Diamond, 1994). Indeed, in the two-dimensional case there is an exact result due to Zeldovich (1957),

$$\langle \bar{\mathbf{B}}^2 \rangle = R_m^{-1} \langle \mathbf{b}^2 \rangle \quad (2\text{-dimensional case}). \quad (12)$$

This result has also been derived in three dimensions using first order smoothing (Krause and Rädler, 1980), but it is important to realize that this result can break down in the nonlinear case in three dimensions, where (11) is in good agreement with the simulation results. However, the assumption of periodic or closed boundaries is an essential one. We return to the more general case in Sects 4.4–4.5.

The time dependence near the saturated state can be approximated by using

$$\langle \bar{\mathbf{J}} \cdot \bar{\mathbf{B}} \rangle \approx k_m^2 \langle \bar{\mathbf{A}} \cdot \bar{\mathbf{B}} \rangle \quad \text{and} \quad \langle \mathbf{j} \cdot \mathbf{b} \rangle \approx k_f^2 \langle \mathbf{a} \cdot \mathbf{b} \rangle. \quad (13)$$

These equations are still valid in the case of fractional helicity (BB02). Only the two-scale assumption is required. Near saturation,

$$|\langle \bar{\mathbf{A}} \cdot \bar{\mathbf{B}} \rangle| = \left( \frac{k_f}{k_m} \right)^2 \langle \mathbf{a} \cdot \mathbf{b} \rangle, \quad (14)$$

i.e.  $|\langle \bar{\mathbf{A}} \cdot \bar{\mathbf{B}} \rangle| \gg |\langle \mathbf{a} \cdot \mathbf{b} \rangle|$  and so we can neglect  $\langle \mathbf{a} \cdot \mathbf{b} \rangle$ , and the magnetic helicity equation (6) becomes therefore an approximate evolution equation for the magnetic helicity of the mean field,

$$\frac{\partial}{\partial t} \langle \bar{\mathbf{A}} \cdot \bar{\mathbf{B}} \rangle = -2\eta\mu_0 \langle \bar{\mathbf{J}} \cdot \bar{\mathbf{B}} \rangle - 2\eta\mu_0 \langle \mathbf{j} \cdot \mathbf{b} \rangle, \quad (15)$$

or, by using (10),

$$k_m^{-1} \frac{\partial}{\partial t} \langle \bar{\mathbf{B}}^2 \rangle = -2\eta k_m \langle \bar{\mathbf{B}}^2 \rangle + 2\eta k_f \langle \mathbf{b}^2 \rangle. \quad (16)$$

Note the plus sign in front of the  $\langle \mathbf{b}^2 \rangle$  term resulting from (10). The plus sign leads to growth while the minus sign in front of the  $\langle \overline{\mathbf{B}}^2 \rangle$  term leads to saturation (but both terms are proportional to the microscopic value of  $\eta$ ; see below). Once the small-scale field has saturated, which will happen after a few dynamical time scales such that  $\langle \mathbf{b}^2 \rangle \approx B_{\text{eq}}^2 \equiv \mu_0 \langle \rho \mathbf{u}^2 \rangle$ , the large-scale field will continue to evolve slowly according to

$$\langle \overline{\mathbf{B}}^2 \rangle = \frac{k_f}{k_m} \langle \mathbf{b}^2 \rangle \left[ 1 - e^{-2\eta k_m^2 (t - t_{\text{sat}})} \right], \quad (17)$$

where  $t_{\text{sat}}$  is the time at which  $\langle \mathbf{b}^2 \rangle$  has reached approximate saturation. In practice,  $t_{\text{sat}}$  can be determined such that (17) describes the simulation data best. We refer to (17) as the *magnetic helicity constraint*. The agreement between this and the actual simulations (Fig. 3) is quite striking.

The significance of this remarkable and simple equation and the almost perfect agreement with simulations is that the constraint can be extrapolated to large values of  $R_m$  where it would provide a benchmark, against which all analytic dynamo theories, when subjected to the same periodic boundary conditions, should be compared to. In particular the late saturation behavior should be equally slow. We return to this in Sect. 5.

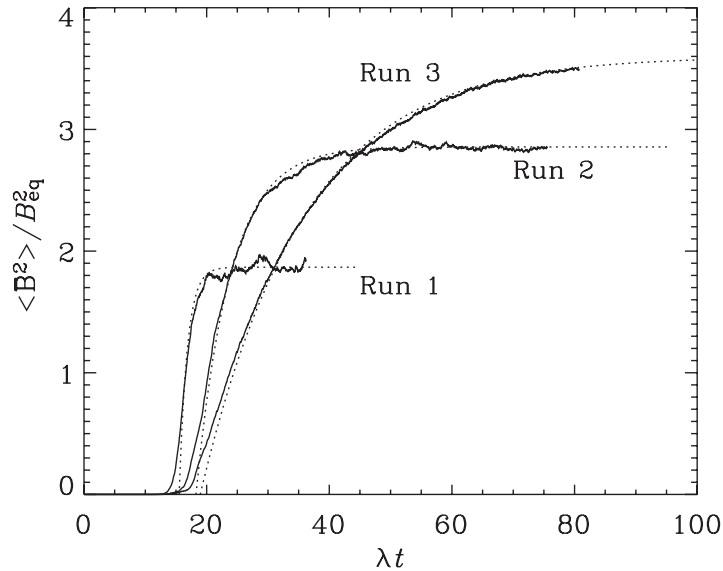


**Fig. 3.** Late saturation phase of fully helical turbulent dynamos for three different values of the magnetic Reynolds number:  $R_m \equiv u_{\text{rms}}/\eta k_f = 2.4, 6,$  and  $18$  for Runs 1, 2, and 3 respectively; see B01. The mean magnetic field,  $\overline{\mathbf{B}}$ , is normalized with respect to the equipartition value,  $B_{\text{eq}} = \sqrt{\mu_0 \rho_0} u_{\text{rms}}$ , and time is normalized with respect to the kinematic growth rate,  $\lambda$ . The dotted lines represent the fit formula (17) which tracks the simulation results rather well [Adapted from [Brandenburg et al. \(2003\)](#)]

An important question is whether anything can be learned about stars and galaxies. Before this can be addressed, we need to understand the differences between dynamos in real astrophysical bodies and dynamos in periodic domains.

## 4 What Do Stars and Galaxies Do Differently?

We begin with a discussion of fractional helicity, shear and other effects that cause the magnetic helicity to be reduced. We then address the possibility of helicity fluxes through boundaries, which can alleviate the helicity constraint (Blackman and Field, 2000).

### 4.1 Fractional Helicity

When the turbulence is no longer fully helical, (10) is no longer valid and needs to be generalized to

$$\langle \bar{\mathbf{J}} \cdot \bar{\mathbf{B}} \rangle = \epsilon_m k_m \langle \bar{\mathbf{B}}^2 \rangle \quad \text{and} \quad \langle \mathbf{j} \cdot \mathbf{b} \rangle = -\epsilon_f k_f \langle \mathbf{b}^2 \rangle, \quad (18)$$

where  $\epsilon_m < 1$  and  $\epsilon_f < 1$  are coefficients denoting the degree to which the mean and fluctuating fields are helical. Equation (13) is still approximately valid in the fractionally helical case.

Maron and Blackman (2002) found that there is a certain threshold of  $\epsilon_f$  below which the large-scale dynamo effect stops working. Qualitatively, this could be understood by noting that the large scale magnetic field comes from the helical part of the flow, so the velocity field can be thought of as having a helical and a nonhelical component, i.e.

$$\mathbf{U} = \mathbf{U}_{\text{hel}} + \mathbf{U}_{\text{nohel}}. \quad (19)$$

However, the dynamo effect has to compete with turbulent diffusion which comes from both the helical and the nonhelical parts of the flow. Thus, when  $|\mathbf{U}_{\text{nohel}}|$  becomes too large compared with  $|\mathbf{U}_{\text{hel}}|$  the large-scale dynamo effect will stop working.

Although we have not yet discussed mean-field theory we may note that the value of the threshold can be understood quantitatively (Brandenburg et al., 2002), hereafter BDS02) and one finds that large-scale dynamo action is only possible when

$$\epsilon_f > \frac{k_m}{k_f} \quad (\text{for large-scale dynamos}). \quad (20)$$

In many three-dimensional turbulence simulations or in astrophysical bodies, this threshold criterion may not be satisfied, and so mean-field dynamo of the type described above ( $\alpha^2$  dynamo) may not be excited. If there is shear, however, this criterion will be modified to

$$\epsilon_f > \epsilon_m \frac{k_m}{k_f}, \quad (21)$$

where  $\epsilon_f$  is the degree to which the large-scale field is helical. In dynamos with strong shear,  $|\epsilon_f|$  may be very small, making mean-field dynamo action in fractionally helical flows more likely. This will be discussed in the next section.

## 4.2 Dynamos with Shear

In the presence of shear, the streamwise component of the field can be amplified by winding up the poloidal (cross-stream) field. Again, the resulting saturation field strength can be estimated based on magnetic helicity conservation arguments.

Note first of all that for closed or periodic domains, (8) is still valid and therefore  $\langle \bar{\mathbf{J}} \cdot \bar{\mathbf{B}} \rangle = -\langle \mathbf{j} \cdot \mathbf{b} \rangle$  in the steady state.<sup>4</sup> However, while  $\langle \mathbf{j} \cdot \mathbf{b} \rangle$  still depends on the helicity of the small-scale field, the corresponding value of  $\langle \bar{\mathbf{J}} \cdot \bar{\mathbf{B}} \rangle$  no longer provides such a stringent bound on  $\langle \bar{\mathbf{B}}^2 \rangle$  as before. This is because shear can amplify the toroidal field independently of any magnetic helicity considerations. The component of  $\bar{\mathbf{B}}^2$  that is amplified by shear is nonhelical and so we have

$$\epsilon_m = |\langle \bar{\mathbf{J}} \cdot \bar{\mathbf{B}} \rangle| / \left( k_m \langle \bar{\mathbf{B}}^2 \rangle \right) \ll 1 \quad (22)$$

(or at least  $|\epsilon_m| \ll 1$  when the helicity of the forcing is negative and  $\epsilon_m$  therefore negative). The value of  $\epsilon_m$  is proportional to the ratio of poloidal to toroidal field

$$\epsilon_m \approx \pm 2 \langle B_{\text{pol}}^2 \rangle^{1/2} / \langle B_{\text{tor}}^2 \rangle^{1/2}, \quad (23)$$

where the numerical pre-factor can be different for different examples.<sup>5</sup> With these preparations the magnetic helicity constraint can be generalized to

$$2B_{\text{pol}}^{\text{rms}} B_{\text{tor}}^{\text{rms}} \approx \frac{k_f}{k_m} \langle \mathbf{b}^2 \rangle \left[ 1 - e^{-2\eta k_m^2 (t - t_{\text{sat}})} \right]. \quad (24)$$

This form of the constraint was proposed and confirmed using three-dimensional simulations of forced helical turbulence with large-scale shear (Brandenburg et al., 2001, hereafter BBS01); see also Fig. 4.

The main conclusion to be drawn from this is that the magnetic helicity constraint is still valid in the presence of shear, i.e. the timescale of saturation is still controlled by the microscopic magnetic diffusivity. The only difference is that stronger field strengths are now possible.

Another interesting aspect is that dynamos with shear allow for oscillatory solutions of the magnetic field. This is expected from mean-field dynamo theory (Steenbeck and Krause, 1969a,b), but it is also borne out by simulations (BBS01). The main result is that the resulting cycle frequency seems to scale with the microscopic magnetic diffusivity, not the turbulent magnetic diffusivity. This confirms again that in a closed domain the magnetic helicity constraint plays a crucial role in controlling the timescale of nonlinear dynamos.

## 4.3 Hall Effect Dynamos

In recent years the importance of the Hall effect has been emphasized by a number of groups, especially in applications to protostellar accretion discs (Balbus and

<sup>4</sup> This is because in the  $\mathbf{E} \cdot \mathbf{B}$  term in the magnetic helicity equation the induction term,  $\mathbf{U} \times \mathbf{B}$ , drops out after dotting with  $\mathbf{B}$ . (For this reason, also ambipolar diffusion and the Hall effect do not change magnetic helicity conservation.)

<sup>5</sup> Take as an example  $\bar{\mathbf{B}}(z) = (\bar{B}_{\text{pol}}, \bar{B}_{\text{tor}}, 0)^T = (\epsilon \cos k_1 z, \sin k_1 z, 0)^T$  for  $\epsilon \ll 1$ , so  $\langle \bar{\mathbf{B}}^2 \rangle \approx 1/2$  and  $\langle \bar{\mathbf{J}} \cdot \bar{\mathbf{B}} \rangle \approx \epsilon k_1$  and therefore  $\epsilon_m = 2\epsilon$ .

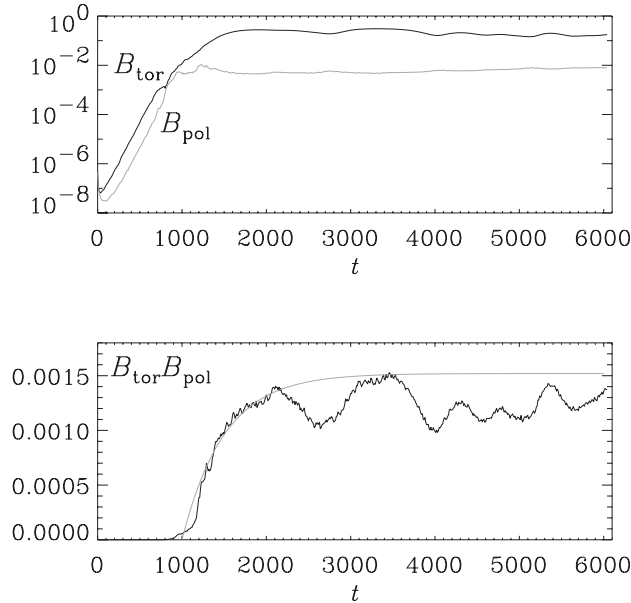


**Fig. 4.** Growth of poloidal and toroidal magnetic fields on a logarithmic scale (*upper panel*), and product of poloidal and toroidal magnetic fields on a linear scale. For the fit we have used  $k_1^2 = 2$ ,  $B_{\text{eq}} = 0.035$ , and  $\epsilon_0 = 1.3$  [Adapted from BBS01]

Terquem, 2001). The hall effect can lead to strong nonlinear steepening of field gradients (Vainshtein et al., 2000), and is therefore important for fast reconnection (e.g. Rogers et al., 2001), which in turn is relevant for neutron stars (Hollerbach and Rüdiger, 2004). Nevertheless, since magnetic helicity generation (and removal) is proportional to the dot product of electric and magnetic fields, and since the Hall current is proportional to  $\mathbf{J} \times \mathbf{B}$ , the Hall term does not affect magnetic helicity conservation. Therefore the resistively limited saturation behavior should not be affected by the Hall term. Nevertheless, some degree of extra field amplification of the large-scale field has been reported (Mininni et al., 2003), and it will be interesting to identify exactly the processes that led to this amplification.

#### 4.4 Magnetic Helicity Exchange Across the Equator or with Depth

The presence of an equator provides a source of magnetic helicity exchange between domains of negative helicity in the northern hemisphere (upper disc plane in an accretion disc) and positive helicity in the southern hemisphere (lower disc plane). A similar situation can also arise in convection zones where the helicity is expected to change with depth (Yoshimura, 1975).

So far, simulations have not yet shown that the losses of small-scale magnetic fields are actually stronger than those of large-scale fields. In Fig. 5 we show the saturation behavior of a system that is periodic, but the helicity of the forcing is

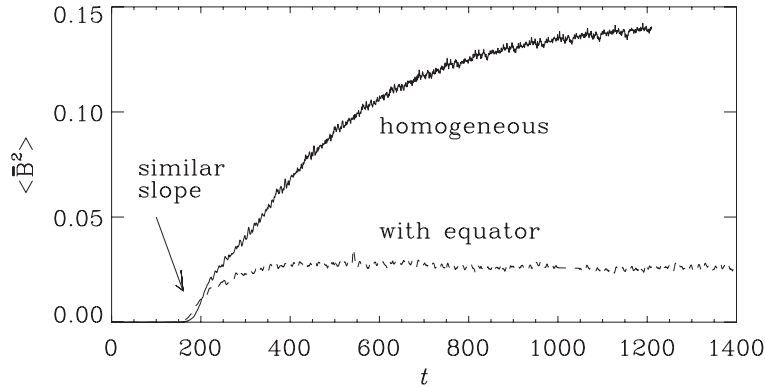


**Fig. 5.** Evolution of the magnetic energy for a run with homogeneous forcing function (*solid line*) and a forcing function whose helicity varies sinusoidally throughout the domain (*dotted line*) simulating the effects of equators at the two nodes of the sinusoidal helicity profile [Adapted from [Brandenburg et al. \(2001\)](#)]

modulated in the  $z$ -direction such that the sign of the kinetic helicity changes in the middle. One can therefore view this system as two subsystems with a boundary in between. This boundary would correspond to the equator in a star or the midplane in a disc. It can also model the change of sign of helicity at some depth in a convection zone.

As far as the magnetic helicity constraint is concerned, the divergence term of current helicity flux is likely to be important when there is a boundary between two domains with different helicities. Naively, one might expect there to be current helicity fluxes that are proportional to the current helicity gradient, analogous to Fick's diffusion law. These current helicity fluxes should be treated separately for large and small-scale components of the field, so we introduce approximations to the current helicity fluxes from the mean and fluctuating fields as

$$\overline{\mathcal{F}}_m \approx -\eta_m \nabla C_m, \quad \overline{\mathcal{F}}_f \approx -\eta_f \nabla C_f. \quad (25)$$

The rate of magnetic helicity loss is here proportional to some turbulent diffusivity coefficient,  $\eta_m$  or  $\eta_f$  for the losses from mean or fluctuating parts, respectively. We assume that the small and large-scale fields are maximally helical (or have known helicity fractions  $\epsilon_m$  and  $\epsilon_f$ ) and have opposite signs of magnetic helicity at small and large scales. The details can be found in BDS02 and [Blackman and Brandenburg \(2003\)](#). The strength of this approach is that it is quite independent of mean-field theory.

We proceed analogously to the derivation of (17) where we used the magnetic helicity equation (6) for a closed domain to estimate the time derivative of the magnetic helicity of the mean field by neglecting the time derivative of the fluctuating field. This is a good approximation after the fluctuating field has reached saturation, i.e.  $t > t_{\text{sat}}$ . Thus, we have

$$k_m^{-1} \frac{\partial}{\partial t} \overline{\mathbf{B}}^2 = -2\eta_m k_m \overline{\mathbf{B}}^2 + 2\eta_f k_f \overline{\mathbf{b}}^2, \quad (26)$$

where  $\eta_m = \eta_f = \eta$  corresponds to the case of a closed domain. Note also that we have here ignored the volume integration, so we are dealing with horizontal averages that depend still on height and on time.

After the time when the small-scale magnetic field saturates, i.e. when  $t > t_{\text{sat}}$ , we have  $\langle \mathbf{b}^2 \rangle \approx \text{constant}$ . After that time, (26) can be solved to give

$$\langle \overline{\mathbf{B}^2} \rangle = \langle \mathbf{b}^2 \rangle \frac{\eta_f k_f}{\eta_m k_m} \left[ 1 - e^{-2\eta_m k_m^2 (t - t_{\text{sat}})} \right], \quad \text{for } t > t_{\text{sat}}. \quad (27)$$

This equation demonstrates three remarkable properties (Brandenburg et al., 2003; Brandenburg and Subramanian, 2005):

- Large-scale helicity losses are needed ( $\eta_m > \eta$ ) to shorten the typical time scale. This is required to prevent resistively long cycle periods.
- However, the saturation amplitude is proportional to  $\eta_f/\eta_m$ , so the large-scale field becomes weaker as  $\eta_m$  is increased. Thus,
- also small-scale losses are needed to prevent the saturation amplitude from becoming too small.

Future work can hopefully verify that these conditions are indeed obeyed by a working large-scale dynamo. Simulations without shear have been unsuccessful to demonstrate that small-scale losses are important (Brandenburg and Dobler, 2001), but new simulations with shear now begin to show significant small-scale losses of current helicity, an enhanced  $\alpha$  effect (Brandenburg and Sandin, 2004), and strong large-scale dynamo action (see below).

#### 4.5 Open Surfaces and Shear

The presence of an outer surface is in many respects similar to the presence of an equator. In both cases one expects magnetic and current helicity fluxes via the divergence term. A particularly instructive system is helical turbulence in an infinitely extended horizontal slab with stress-free boundary conditions and a vertical field condition, i.e.

$$u_{x,z} = u_{y,z} = u_z = B_x = B_y = 0. \quad (28)$$

Such simulations have been performed by Brandenburg and Dobler (2001) who found that a mean magnetic field is generated, similar to the case with periodic boundary conditions, but that the energy of the mean magnetic field,  $\langle \overline{\mathbf{B}^2} \rangle$ , decreases with magnetic Reynolds number. Nevertheless, the energy of the total magnetic field,  $\langle \mathbf{B}^2 \rangle$ , does not decrease with increasing magnetic Reynolds number. Although they found that  $\langle \overline{\mathbf{B}^2} \rangle$  decreases only like  $R_m^{-1/2}$ , new simulations confirm that a proper scaling regime has not yet been reached and that the current data may well be compatible with an  $R_m^{-1}$  dependence; see Fig. 6.

Clearly, an asymptotic decrease of the mean magnetic field must mean that the small-scale dynamo does not work with such boundary conditions. Thus, the anticipated advantages of open boundary conditions are not borne out by this type of simulations.

At this point we can mention some new simulations in a cartesian domain where differential rotation has been modeled as a region of the convection zone without explicitly allowing for convection; see Fig. 7. Instead, an external forcing term has

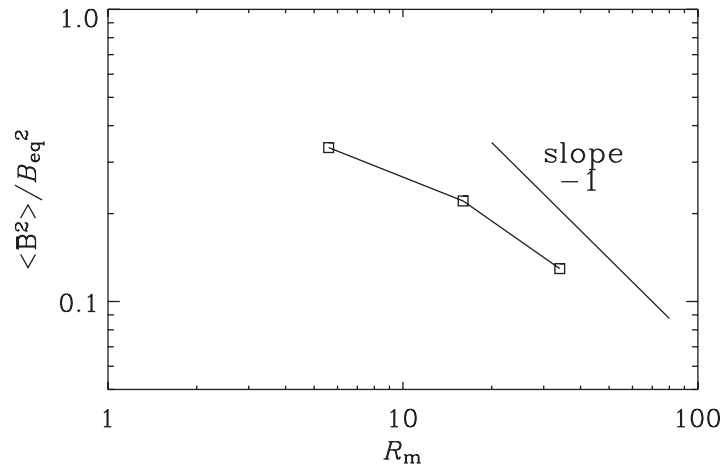


**Fig. 6.** Dependence of the energy of the mean magnetic field on the magnetic Reynolds number for a run with open boundary conditions and no shear

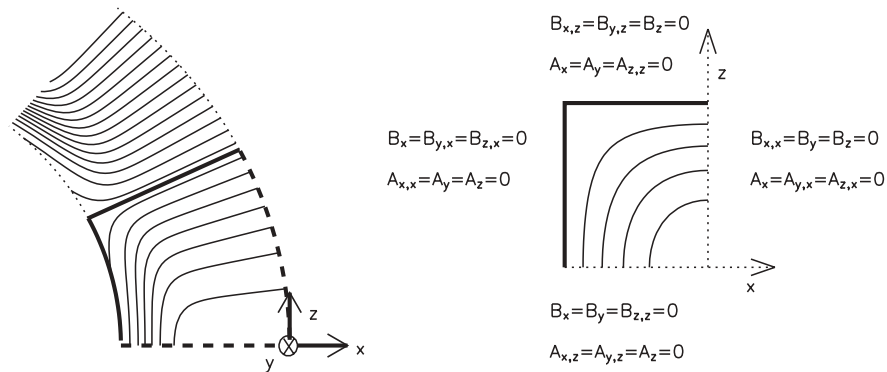


**Fig. 7.** *Left:* A sketch of the solar angular velocity at low latitudes with spoke-like contours in the bulk of the convection zone merging gradually into uniform rotation in the radiative interior. The low latitude region, modeled in this paper, is indicated by thick lines. *Right:* Differential rotation in our cartesian model, with the equator being at the bottom, the surface to the right, the bottom of the convection zone to the left and mid-latitudes at the top [Adapted from [Brandenburg and Sandin \(2004\)](#)]

been applied that also drives the differential rotation. (Studies of the  $\alpha$  effect have already been published; see Sect. 5.6 for details of the simulations and Sect. 5 for a discussion of the direct correspondence between the helicity constraint and the so-called catastrophic  $\alpha$  quenching.) Here we briefly report on recent explicit dynamo simulations that have been carried out in this geometry.

The size of the computational domain is  $\frac{1}{2}\pi \times 2\pi \times \frac{1}{2}\pi$  and the numerical resolution is  $128 \times 512 \times 128$  meshpoints. The magnetic Reynolds number based on

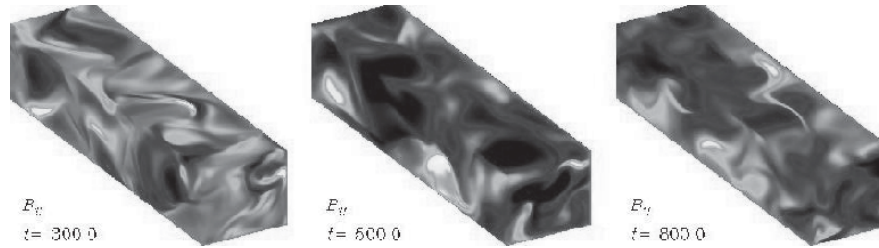


**Fig. 8.** Visualization of the toroidal magnetic field during three different times during the growth and saturation for the run without kinetic helicity

the forcing wavenumber and the turbulent flow is around 80 and shear flow velocity exceeds the rms turbulent velocity by a factor of about 5. We have carried out experiments with no helicity in the forcing (labeled by  $\alpha = 0$ ), as well as positive and negative helicity in the forcing (labeled by  $\alpha < 0$  and  $\alpha > 0$ , respectively); see Fig. 8 for a visualization of the run without kinetic helicity. We emphasize that no explicit  $\alpha$  effect has been invoked. The labeling just reflects the fact that, in isotropic turbulence, negative kinetic helicity (as in the northern hemisphere of a star or the upper disc plane in galaxies) leads to a positive  $\alpha$  effect, and vice versa.

We characterize the relative strength of the mean field by the ratio  $q = \langle \overline{B^2} \rangle / \langle B^2 \rangle$ , where overbars denote an average in the toroidal ( $y$ ) direction; see Fig. 9. There are two surprising results emerging from this work. First, in the presence of shear rather strong mean fields can be generated, where up to 70% of the energy can be in the mean field; see Fig. 9. Second, even without any kinetic helicity in the flow there is strong large-scale field generation. Obviously, this cannot be an

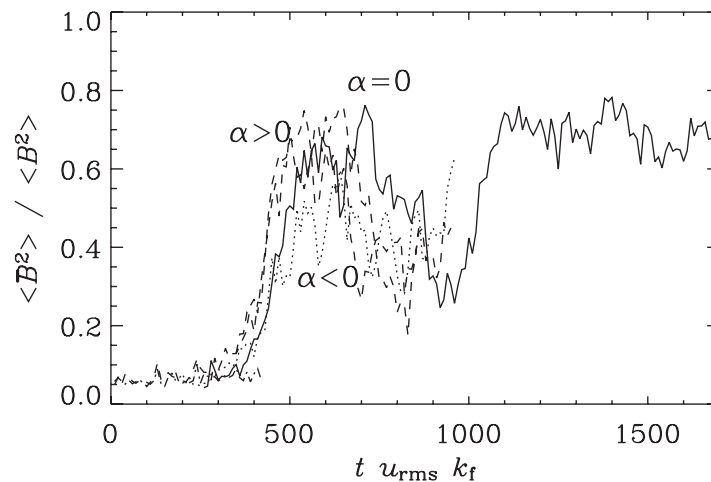


**Fig. 9.** Saturation behavior of the ratio  $q = \langle \overline{B^2} \rangle / \langle B^2 \rangle$  for runs with different kinetic helicity of the flow. *Solid line*: zero helicity, *dotted line*: positive helicity (opposite to the sun) *dashed line*: negative helicity (as in the sun)

$\alpha\Omega$  dynamo in the usual sense. One possibility is the  $\delta \times \mathbf{J}$  effect, which emerged originally in the presence of the Coriolis force; see Rädler (1969) and Krause and Rädler (1980). In the present case with no Coriolis force, however, a  $\delta \times \mathbf{J}$  effect is possible even in the presence of shear alone, because the vorticity associated with the shear contributes directly to  $\delta \propto \overline{\mathbf{W}} = \nabla \times \overline{\mathbf{U}}$  (Rogachevskii and Kleeorin, 2003).

There is evidence that the strong dynamo action seen in the simulations is only possible due to the combined presence of open boundaries and shear. This however has so far only been checked explicitly for the  $\alpha$  effect that is present when the forcing is helical; see Sect. 5.6. In the case of the solar surface such losses are actually observed to occur in the form of coronal mass ejections and in active regions. In the sun, coronal mass ejections are quite vigorous events that are known to shed large amounts of helical magnetic fields (Berger and Ruzmaikin, 2000; DeVore, 2000; Chae, 2000; Low, 2001). This kind of physics is not at all represented by adopting vacuum or pseudo-vacuum (vertical field) boundary conditions, as was done in Brandenburg and Subramanian (2005).

## 5 Connection with the $\alpha$ Effect

### 5.1 Preliminary Considerations

The  $\alpha$  effect formalism provides so far the only workable mathematical framework for describing the large-scale dynamo action seen in simulations of helically forced turbulence. (In this section we retain the  $\mu_0$  factor.) The governing equation for the mean magnetic field is

$$\frac{\partial \overline{\mathbf{B}}}{\partial t} = \nabla \times (\overline{\mathbf{U}} \times \overline{\mathbf{B}} + \overline{\boldsymbol{\mathcal{E}}} - \eta\mu_0 \overline{\mathbf{J}}), \quad (29)$$

where  $\overline{\boldsymbol{\mathcal{E}}} = \overline{\mathbf{u} \times \mathbf{b}}$  is the electromotive force resulting from the  $\mathbf{u} \times \mathbf{b}$  nonlinearity in the averaged Ohm's law. Without mean flow,  $\overline{\mathbf{U}} = 0$ , and an electromotive force given by a homogeneous isotropic  $\alpha$  effect and turbulent diffusion  $\eta_t$ , i.e.

$$\overline{\boldsymbol{\mathcal{E}}} = \alpha \overline{\mathbf{B}} - \eta_t \mu_0 \overline{\mathbf{J}}, \quad (30)$$

we have

$$\frac{\partial \overline{\mathbf{B}}}{\partial t} = \alpha \nabla \times \overline{\mathbf{B}} + (\eta + \eta_t) \nabla^2 \overline{\mathbf{B}}, \quad (31)$$

which has solutions of the form  $\overline{\mathbf{B}} = \hat{\mathbf{B}} e^{i\mathbf{k} \cdot \mathbf{x} + \lambda t}$  with the dispersion relation

$$\lambda_{\pm} = -\eta_{\Gamma} k^2 \pm |\alpha k|, \quad (32)$$

and three possible eigenfunctions (appropriate for the periodic box)

$$\overline{\mathbf{B}}(\mathbf{x}) = \begin{pmatrix} \cos k_m z \\ \sin k_m z \\ 0 \end{pmatrix}, \quad \begin{pmatrix} 0 \\ \cos k_m x \\ \sin k_m x \end{pmatrix}, \quad \text{or} \quad \begin{pmatrix} \sin k_m y \\ 0 \\ \cos k_m y \end{pmatrix}, \quad (33)$$

where  $k_m = k_1 = 1$ . Obviously, when the coefficients  $\alpha$  and  $\eta_{\Gamma} \equiv \eta + \eta_t$  remain constant, and there is an exponentially growing solution (for  $|\alpha| > \eta_{\Gamma} k_1$ ), the

solution must eventually grow beyond any bound. At the latest when the magnetic field reaches equipartition with the kinetic energy,  $\alpha$  and  $\eta_t$  must begin to depend on the magnetic field itself. However, the present case is sufficiently simple so that we can continue to assume that  $\overline{\mathbf{B}}^2$ , as well as  $\alpha$  and  $\eta_t$ , are uniform in space and depend only on time.

Comparison with simulations has enabled us to eliminate a large number of various quenching models where  $\alpha = \alpha(\overline{\mathbf{B}})$ . The only quenching model that seems reasonably well compatible with simulations of  $\alpha^2$ -like dynamo action in a periodic box *without* shear is

$$\alpha = \frac{\alpha_0}{1 + R_m \overline{\mathbf{B}}^2 / B_{\text{eq}}^2}, \quad \eta_t = \frac{\eta_{t0}}{1 + R_m \overline{\mathbf{B}}^2 / B_{\text{eq}}^2} \quad (\text{empirical}), \quad (34)$$

see Fig. 3. However, this type of quenching is not fully compatible with magnetic helicity conservation, as has been shown by [Field and Blackman \(2002\)](#). This will be discussed in the next section.

## 5.2 Dynamical $\alpha$ Quenching

The basic idea is that magnetic helicity conservation must be obeyed, but the presence of an  $\alpha$  effect leads to magnetic helicity of the mean field which has to be balanced by magnetic helicity of the fluctuating field. This magnetic helicity of the fluctuating (small-scale) field must be of opposite sign to that of the mean (large-scale) field.

We begin with the uncurled mean-field induction equation, written in the form

$$\frac{\partial \overline{\mathbf{A}}}{\partial t} = \overline{\boldsymbol{\mathcal{E}}} - \eta \mu_0 \overline{\mathbf{J}}, \quad (35)$$

dot it with  $\overline{\mathbf{B}}$ , add the result to  $\overline{\mathbf{A}} \cdot \partial \overline{\mathbf{B}} / \partial t$ , average over the periodic box, and obtain

$$\frac{\partial}{\partial t} \langle \overline{\mathbf{A}} \cdot \overline{\mathbf{B}} \rangle = 2 \langle \overline{\boldsymbol{\mathcal{E}}} \cdot \overline{\mathbf{B}} \rangle - 2 \eta \mu_0 \langle \overline{\mathbf{J}} \cdot \overline{\mathbf{B}} \rangle. \quad (36)$$

To satisfy the helicity equation for the full field,  $\langle \mathbf{A} \cdot \mathbf{B} \rangle = \langle \overline{\mathbf{A}} \cdot \overline{\mathbf{B}} \rangle + \langle \mathbf{a} \cdot \mathbf{b} \rangle$ , we must have

$$\frac{\partial}{\partial t} \langle \mathbf{a} \cdot \mathbf{b} \rangle = -2 \langle \overline{\boldsymbol{\mathcal{E}}} \cdot \overline{\mathbf{B}} \rangle - 2 \eta \mu_0 \langle \mathbf{j} \cdot \mathbf{b} \rangle. \quad (37)$$

Note the minus sign in front of the  $2 \langle \overline{\boldsymbol{\mathcal{E}}} \cdot \overline{\mathbf{B}} \rangle$  term, indicating once again that the  $\alpha$  effect produces magnetic helicity of opposite sign at the mean and fluctuating fields. The sum of the two equations yields (6).

The significance of (37) is that it contains the  $\langle \mathbf{j} \cdot \mathbf{b} \rangle$  term which contributes to the  $\alpha$  effect, as was first shown by [Pouquet et al. \(1976\)](#). Specifically, they found (see also [Blackman and Field, 2002](#))

$$\alpha = \alpha_K + \alpha_M, \quad \text{with} \quad \alpha_K = -\frac{1}{3} \tau \langle \boldsymbol{\omega} \cdot \mathbf{u} \rangle, \quad \alpha_M = +\frac{1}{3} \tau \langle \mathbf{j} \cdot \mathbf{b} \rangle, \quad (38)$$

where  $\tau$  is the correlation time of the turbulence,  $\boldsymbol{\omega} = \nabla \times \mathbf{u}$  is the vorticity, and  $\langle \boldsymbol{\omega} \cdot \mathbf{u} \rangle$  is the kinematic helicity.

Using  $\langle \mathbf{j} \cdot \mathbf{b} \rangle \approx k_f^2 \langle \mathbf{a} \cdot \mathbf{b} \rangle$ , see (13), we can rewrite (37) in a form that can directly be used in mean-field calculations:

$$\frac{d\alpha}{dt} = -2\eta_t k_f^2 \left( \frac{\alpha \langle \overline{\mathbf{B}^2} \rangle - \eta_t \langle \overline{\mathbf{J} \cdot \mathbf{B}} \rangle}{B_{\text{eq}}^2} + \frac{\alpha - \alpha_K}{R_m} \right), \quad (39)$$

Here we have used  $\eta_t = \frac{1}{3}\tau u_{\text{rms}}^2$  to eliminate  $\tau$  in favor of  $\eta_t$  and  $B_{\text{eq}}^2 = \mu_0 \rho_0 u_{\text{rms}}^2$  to eliminate  $u_{\text{rms}}^2$  in favor of  $B_{\text{eq}}^2$ .

So,  $\alpha$  is no longer just an algebraic function of  $\overline{\mathbf{B}}$ , but it is related to  $\overline{\mathbf{B}}$  via a *dynamical*, explicitly time-dependent equation. In the context of dynamos in periodic domains, where magnetic helicity conservation is particularly important, the time dependence of  $\alpha$  can hardly be ignored, unless one wants to describe the final stationary state, which can be at the end of a very slow saturation phase. However, in order to make contact with earlier work, it is useful to consider the stationary limit of (39), i.e. set  $\partial\alpha/\partial t$ .

### 5.3 Steady Limit and its Limitations

In the steady limit the term in brackets in (39) can be set to zero, so this equation reduces to

$$R_m \frac{\alpha \langle \overline{\mathbf{B}^2} \rangle - \eta_t \langle \overline{\mathbf{J} \cdot \mathbf{B}} \rangle}{B_{\text{eq}}^2} + \alpha = \alpha_K \quad (\text{for } d\alpha/dt = 0). \quad (40)$$

Solving this equation for  $\alpha$  yields (Kleeorin et al., 1982; Gruzinov and Diamond, 1994)

$$\alpha = \frac{\alpha_K + \eta_t R_m \langle \overline{\mathbf{J} \cdot \mathbf{B}} \rangle / B_{\text{eq}}^2}{1 + R_m \langle \overline{\mathbf{B}^2} \rangle / B_{\text{eq}}^2} \quad (\text{for } d\alpha/dt = 0). \quad (41)$$

And, sure enough, for the numerical experiments with an imposed large scale field over the scale of the box (Cattaneo and Hughes, 1996), where  $\overline{\mathbf{B}}$  is spatially uniform and therefore  $\overline{\mathbf{J}} = 0$ , one recovers the ‘catastrophic’ quenching formula,

$$\alpha = \frac{\alpha_K}{1 + R_m \langle \overline{\mathbf{B}^2} \rangle / B_{\text{eq}}^2} \quad (\text{for } \overline{\mathbf{J}} = 0), \quad (42)$$

which implies that  $\alpha$  becomes quenched when  $\langle \overline{\mathbf{B}^2} \rangle / B_{\text{eq}}^2 = R_m^{-1} \approx 10^{-8}$  for the sun, and for even smaller fields in the case of galaxies.

On the other hand, if the mean field is not imposed, but maintained by dynamo action,  $\overline{\mathbf{B}}$  cannot be spatially uniform and then  $\overline{\mathbf{J}}$  is finite. In the case of a Beltrami field (33),  $\langle \overline{\mathbf{J} \cdot \mathbf{B}} \rangle / \langle \overline{\mathbf{B}^2} \rangle \equiv \tilde{k}_m$  is some effective wavenumber of the large-scale field [ $\tilde{k}_m = \epsilon_m k_m$ ; see (22)]. Since  $R_m$  enters both the numerator and the denominator,  $\alpha$  tends to  $\eta_t \tilde{k}_m$ , i.e.

$$\alpha \rightarrow \eta_t \tilde{k}_m \quad (\text{for } \overline{\mathbf{J}} \neq 0 \text{ and } \overline{\mathbf{J}} \parallel \overline{\mathbf{B}}). \quad (43)$$

Compared with the kinematic estimate,  $\alpha_K \approx \eta_t k_f$ ,  $\alpha$  is only quenched by the modified scale separation ratio. More importantly,  $\alpha$  is quenched to a value that is just slightly above the critical value for the onset of dynamo action,  $\alpha_{\text{crit}} = \eta_T \tilde{k}_m$ . How is it then possible that the fit formula (34) for  $\alpha$  and  $\eta_t$  produced reasonable agreement with the simulations? The reason is that in the simple case of an  $\alpha^2$  dynamo the solutions are degenerate in the sense that  $\overline{\mathbf{J}}$  and  $\overline{\mathbf{B}}$  are parallel to each other. Therefore, the term  $\langle \overline{\mathbf{J} \cdot \mathbf{B}} \rangle \overline{\mathbf{B}}$  is the same as  $\langle \overline{\mathbf{B}^2} \rangle \overline{\mathbf{J}}$ , which means that in the mean EMF the term  $\alpha \overline{\mathbf{B}}$ , where  $\alpha$  is given by (41), has a component that can

be expressed as being parallel to  $\bar{\mathbf{J}}$ . In other words, the roles of turbulent diffusion (proportional to  $\bar{\mathbf{J}}$ ) and  $\alpha$  effect (proportional to  $\bar{\mathbf{B}}$ ) cannot be disentangled. This is the *force-free degeneracy* of  $\alpha^2$  dynamos in a periodic box (BB02). This degeneracy is also the reason why for  $\alpha^2$  dynamos the late saturation behavior can also be described by an algebraic (non-dynamical, but catastrophic) quenching formula proportional to  $1/(1 + R_m \langle \bar{\mathbf{B}}^2 \rangle)$  for *both*  $\alpha$  and  $\eta_t$ , as was done in B01. To see this, substitute the steady state quenching expression for  $\alpha$ , from (41), into the expression for  $\bar{\mathcal{E}}$ . We find

$$\begin{aligned} \bar{\mathcal{E}} &= \alpha \bar{\mathbf{B}} - (\eta + \eta_t) \bar{\mathbf{J}} = \frac{\alpha_K + R_m \eta_t \langle \bar{\mathbf{J}} \cdot \bar{\mathbf{B}} \rangle / B_{\text{eq}}^2}{1 + R_m \langle \bar{\mathbf{B}}^2 \rangle / B_{\text{eq}}^2} \bar{\mathbf{B}} - \eta_t \bar{\mathbf{J}} \\ &= \frac{\alpha_K \bar{\mathbf{B}}}{1 + R_m \langle \bar{\mathbf{B}}^2 \rangle / B_{\text{eq}}^2} - \frac{\eta_t \bar{\mathbf{J}}}{1 + R_m \langle \bar{\mathbf{B}}^2 \rangle / B_{\text{eq}}^2}, \end{aligned} \quad (44)$$

which shows that in the force-free case the adiabatic approximation, together with constant (unquenched) turbulent magnetic diffusivity, becomes equal to the pair of expressions where both  $\alpha$  and  $\eta_t$  are catastrophically quenched. This force-free degeneracy is lifted in cases with shear or when the large-scale field is no longer fully helical (e.g. in a nonperiodic domain, and in particular in the presence of open boundaries).

#### 5.4 The Keinigs Relation and its Relevance

Applying (37) to the steady state using  $\bar{\mathcal{E}} = \alpha \bar{\mathbf{B}} - \eta_t \mu_0 \bar{\mathbf{J}}$  (and retaining  $\mu_0$  factor), we get

$$\alpha = -\eta_t \mu_0 \frac{\langle \mathbf{j} \cdot \mathbf{b} \rangle}{\langle \bar{\mathbf{B}}^2 \rangle} + \eta_t k_m \quad (\text{for periodic domain}), \quad (45)$$

where we have defined an effective wavenumber of the large-scale field,  $k_m = \mu_0 \langle \bar{\mathbf{J}} \cdot \bar{\mathbf{B}} \rangle / \langle \bar{\mathbf{B}}^2 \rangle$ ; see (9). This relation applies only to a closed or periodic box, because otherwise there would be boundary terms. Moreover, if the mean field is defined as a volume average, i.e.  $\bar{\mathbf{B}} = \langle \mathbf{B} \rangle \equiv \mathbf{B}_0$ , then  $\mu_0 \bar{\mathbf{J}} = \nabla \times \mathbf{B}_0 = 0$ , so  $k_m = 0$  and one has simply

$$\alpha = -\eta_t \mu_0 \frac{\langle \mathbf{j} \cdot \mathbf{b} \rangle}{\langle \bar{\mathbf{B}}^2 \rangle} \quad (\text{for imposed field}). \quad (46)$$

This equation is due to Keinigs (1983). For the more general case with  $k_m \neq 0$  this equation has been discussed in more detail by Brandenburg and Subramanian (2005) and Brandenburg and Matthaeus (2004).

Let us now discuss the significance of this relation relative to (41). Both equations apply only in the strictly steady state, of course. Since we have assumed stationarity, we can replace  $\langle \mathbf{j} \cdot \mathbf{b} \rangle$  by  $-\langle \bar{\mathbf{J}} \cdot \bar{\mathbf{B}} \rangle$ ; see (9). Thus, (45) reduces to

$$\alpha = \eta_T k_m \quad (47)$$

where  $\eta_T = \eta + \eta_t$  is the total (turbulent and microscopic) magnetic diffusivity. This relation is just the condition for a marginally excited dynamo; see (32), so it does *not* produce any independent estimate for the value of  $\alpha$ . In particular, it does not provide a means of independently testing (41). The two can however be used to calculate the mean-field energy in the saturated state and we find (BB02)

$$\frac{\langle \overline{\mathbf{B}}^2 \rangle}{B_{\text{eq}}^2} = \frac{\alpha - \eta_{\Gamma} k_{\text{m}}}{\eta_{\text{t}} k_{\text{m}}} \quad (\text{periodic domain}). \quad (48)$$

By replacing  $k_{\text{m}}$  by an effective value  $\tilde{k}_{\text{m}}$ , this equation can be generalized to apply also to the case with shear (for details see BB02).

### 5.5 Blackman's Multi-scale Model: Application to Helical Turbulence with Imposed Field

The restriction to a two scale model may in some cases turn out to be insufficient to capture the variety of scales involved in astrophysical bodies. This is already important in the kinematic stage when the small-scale dynamo obeys the [Kazantsev \(1968\)](#) scaling with a  $k^{3/2}$  spectrum that peaks at the resistive scale. As the dynamo saturates, the peak moves to the forcing scale. This lead [Blackman \(2003\)](#) to develop a four scale model where he includes, in addition to the wavenumbers of the mean field  $k_{\text{m}}$  ( $\equiv k_1$ ) and the wavenumber of the energy carrying scale of the velocity fluctuations  $k_{\text{f}}$  ( $\equiv k_2$ ), also the viscous wavenumber  $k_{\nu}$  ( $\equiv k_3$ ) and the resistive wavenumber  $k_{\eta}$  ( $\equiv k_4$ ). The set of helicity equations for the four different scales is

$$(\partial_t + 2\eta k_1^2) H_1 = 2\langle \overline{\mathcal{E}}_1 \cdot \overline{\mathbf{B}}_1 \rangle + 2\langle \overline{\mathcal{E}}_2 \cdot \overline{\mathbf{B}}_1 \rangle, \quad (49)$$

$$(\partial_t + 2\eta k_2^2) H_2 = -2\langle \overline{\mathcal{E}}_1 \cdot \overline{\mathbf{B}}_1 \rangle + 2\langle \overline{\mathcal{E}}_2 \cdot \overline{\mathbf{B}}_2 \rangle, \quad (50)$$

$$(\partial_t + 2\eta k_3^2) H_3 = -2\langle \overline{\mathcal{E}}_2 \cdot \overline{\mathbf{B}}_1 \rangle - 2\langle \overline{\mathcal{E}}_2 \cdot \overline{\mathbf{B}}_2 \rangle, \quad (51)$$

$$(\partial_t + 2\eta k_4^2) H_4 = 0, \quad (52)$$

where  $\overline{\mathcal{E}}_1$  is the usual electromotive force based on kinetic helicity at the forcing scale,  $k_2$ , with feedback proportional to  $H_2$ , and  $\overline{\mathcal{E}}_2$  has no kinetic helicity input but only reacts to the automatically generated magnetic helicity  $H_3$  produced at the viscous scale  $k_3$ . These equations are constructed such that

$$\frac{\partial}{\partial t} \sum_{i=1}^4 H_i = -2\eta \sum_{i=1}^4 k_i^2 H_i, \quad (53)$$

which is consistent with the magnetic helicity equation (6) for the total field. An important outcome of this model is that in the limit of large  $R_{\text{m}}$  the magnetic peak travels from  $k_3$  to  $k_2$  on a dynamical timescale, i.e. a timescale that is independent of  $R_{\text{m}}$ .

[Brandenburg and Matthaeus \(2004\)](#) have applied the general idea to the case of a model with an applied field. Here the new scale is the scale of the applied field, but since this scale is infinite, this field is fixed and not itself subject to an evolution equation. Nevertheless, the electromotive force from this field acts as a sink on the next smaller scale with wavenumber  $k_1$ , which is the largest wavenumber in the domain of the simulation. They thus arrive at the following set of evolution equations,

$$\left[ (\partial_t + 2\eta k_0^2) H_0 = \dots + 2\langle \overline{\mathcal{E}}_0 \cdot \overline{\mathbf{B}}_0 \rangle, \right] \quad (54)$$

$$(\partial_t + 2\eta k_1^2) H_1 = -2\langle \overline{\mathcal{E}}_0 \cdot \overline{\mathbf{B}}_0 \rangle + 2\langle \overline{\mathcal{E}}_1 \cdot \overline{\mathbf{B}}_1 \rangle, \quad (55)$$

$$(\partial_t + 2\eta k_2^2) H_2 = -2\langle \overline{\mathcal{E}}_1 \cdot \overline{\mathbf{B}}_1 \rangle. \quad (56)$$

The square brackets around the first equation indicate that this equation is not explicitly included. From the second equation (55) one can see that there is a competition between two opposing effects: the  $\alpha$  effect operating on the imposed field  $\mathbf{B}_0$  and the  $\alpha$  effect operating on the  $\mathbf{B}_1$  field on the scale of the box. When the imposed field exceeds a certain field strength,  $B_0 > B_*$ , the former will dominate, reversing the sign of the magnetic helicity at wavenumber  $k_1$ . This is actually seen in the simulations of helically forced turbulence with an imposed field  $\mathbf{B}_0$ ; see Fig. 10. We return to this at the end of this section.

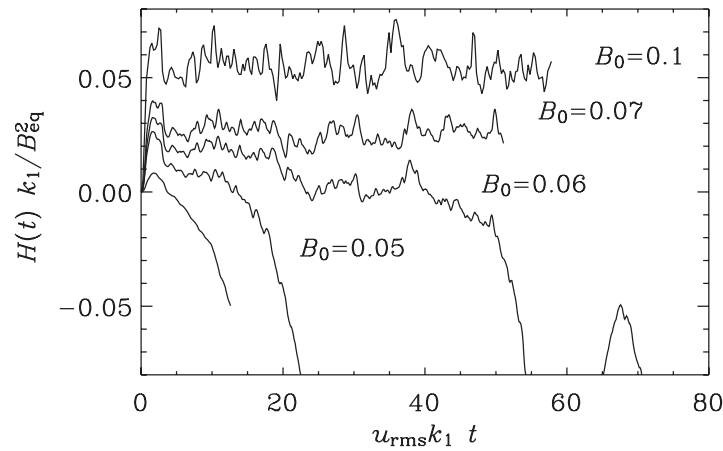


**Fig. 10.** Evolution of the total magnetic helicity,  $H = H_1 + H_{\bar{t}}$ , as a function of  $t$  for different values of  $B_0$ , as obtained from the three-dimensional simulation. Note the change of sign at  $B_0 \approx B_* \approx 0.07$  [Adapted from [Brandenburg and Matthaeus \(2004\)](#)]

The work of [Brandenburg and Matthaeus \(2004\)](#) was motivated by earlier work of [Montgomery et al. \(2002\)](#) and [Milano et al. \(2003\)](#) who showed that, if the imposed magnetic field is weak or absent, there is a strong nonlocal transfer of magnetic helicity and magnetic energy from the forcing scale to larger scales. This leads eventually to the accumulation of magnetic energy at the scale of the box ([Meneguzzi et al., 1981](#); [Balsara and Pouquet, 1999](#), B01). As the strength of the imposed field (wavenumber  $k = 0$ ) is increased, the accumulation of magnetic energy at the scale of the box ( $k = 1$ ) becomes more and more suppressed ([Montgomery et al., 2002](#)).

In order to solve the model equations, we have to make some assumptions about the electromotive force operating at  $k_0$  and  $k_1$ . The large-scale magnetic helicity production from the  $\alpha$  effect operating on the imposed field is  $\mathcal{E}_0 \cdot \mathbf{B}_0 = \alpha_1 \mathbf{B}_0^2$ . On the other hand,  $\mathcal{E}_1$  at wavenumber  $k_1$  is given by

$$\mathcal{E}_1 = \alpha_f \mathbf{B}_1 - \eta_t \mu_0 \mathbf{J}_1. \quad (57)$$

To calculate  $\langle \mathcal{E}_1 \cdot \mathbf{B}_1 \rangle$  in (55) and (56) we dot (57) with  $\mathbf{B}_1$ , volume average, and note that  $\mu_0 \langle \mathbf{J}_1 \cdot \mathbf{B}_1 \rangle = k_1^2 H_1$  and  $\langle \mathbf{B}_1^2 \rangle = k_1 |H_1|$ . The latter relation assumes that

the field at wavenumber  $k_1$  is fully helical, but that it can have either sign. Thus, we have

$$\langle \mathcal{E}_1 \cdot \mathbf{B}_1 \rangle = \alpha_f k_1 |H_1| - \eta_t k_1^2 H_1 . \quad (58)$$

The  $\alpha$  effects on the two scales are proportional to the residual magnetic helicity of Pouquet et al. (1976); see (38). In terms of  $H_1$  and  $H_2 \equiv H_f$  we write

$$\alpha_1 = \alpha_K + \frac{1}{3} \tau k_1^2 H_1 , \quad (59)$$

$$\alpha_2 = \alpha_K + \frac{1}{3} \tau k_2^2 H_2 , \quad (60)$$

for the  $\alpha$  effect with feedback from  $H_1$  and  $H_2$ , respectively.

For finite values of  $B_0$ , the final value of  $H_1$  is particularly sensitive to the value of  $\alpha_K$  and turns out to be too large compared with the simulations. This disagreement with simulations is readily removed by taking into account that  $\alpha_K = -\frac{1}{3} \tau \langle \boldsymbol{\omega} \cdot \mathbf{u} \rangle$  should itself be quenched when  $B_0$  becomes comparable to  $B_{\text{eq}}$ . Thus, we write

$$\alpha_K = \alpha_{K0} / (1 + B_0^2 / B_{\text{eq}}^2) , \quad (61)$$

which is a good approximation to more elaborate expressions (Rüdiger and Kitchatinov, 1993). We emphasize that this equation only applies to  $\alpha_K$  and is therefore distinct from (34), (39), or (41).

Under the assumption that the turbulence is fully helical, the critical value  $B_*$  of the imposed field can be estimated by balancing the two terms on the right hand side of (56) and by approximating,  $\alpha \approx \eta_t k_f$  and  $\langle \mathbf{j} \cdot \mathbf{b} \rangle \approx k_f B_{\text{eq}}^2$ . This yields

$$B_*^2 / B_{\text{eq}}^2 \approx \eta / \eta_t \equiv R_m^{-1} , \quad (62)$$

where the last equality is to be understood as a definition of the magnetic Reynolds number, see also BB02. For  $B_0 > B_*$  the sign of the magnetic helicity is the same both at  $k = 1$  and at  $k = k_f$ , while for  $B_0 < B_*$  the signs are opposite.

In Fig. 11 we show the result of a numerical integration of (55) and (56). Both the three-dimensional simulation and the two-scale model show a similar value of  $B_0 \approx 0.06 \dots 0.07$ , above which  $H_1$  changes sign. This confirms the validity of our estimate of the critical value  $B_*$  obtained from (62). Secondly, the time evolution is slow when  $B_0 < B_*$  and faster when  $B_0 > B_*$ . In the simulation, however, the field attains its final level for  $B_0 > B_*$  almost instantaneously, which is not the case in the model. The significance of this discrepancy remains unclear. Nevertheless, the level of agreement between the simulations and 3-scale model is surprising, suggesting that the approach can indeed be quite useful.

## 5.6 Alpha Effect with Open Boundaries and Shear

In a recent paper, Brandenburg and Sandin (2004) have carried out a range of simulations for different values of the magnetic Reynolds number,  $R_m = u_{\text{rms}} / (\eta k_f)$ , for both open and closed boundary conditions using the geometry depicted on the right hand panel of Fig. 7. In order to measure  $\alpha$ , a uniform magnetic field,  $\mathbf{B}_0 = \text{const}$ , is imposed, and the magnetic field is now written as  $\mathbf{B} = \mathbf{B}_0 + \nabla \times \mathbf{A}$ . They have determined  $\alpha$  by measuring the turbulent electromotive force, and hence  $\alpha = \langle \mathcal{E} \rangle \cdot \mathbf{B}_0 / B_0^2$ . Similar investigations have been done before both for forced turbulence (Cattaneo and Hughes, 1996, B01) and for convective turbulence (Brandenburg et al., 1990; Ossendrijver et al., 2001).

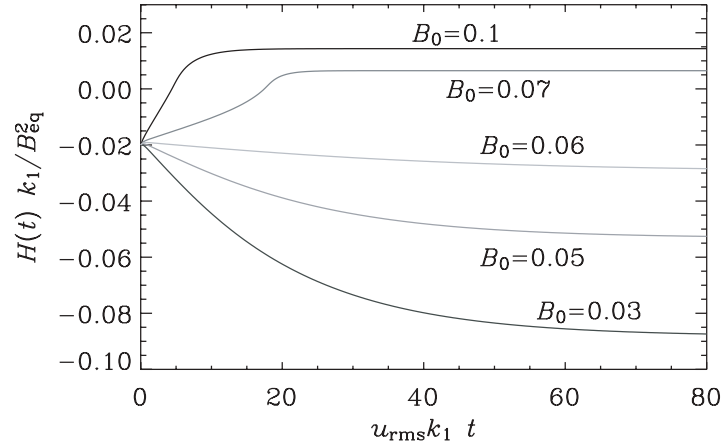


**Fig. 11.** Evolution of magnetic helicity as a function of  $t$  for different values of  $B_0$ , as obtained from the two-scale model [Adapted from [Brandenburg and Matthaeus \(2004\)](#)]

As expected,  $\alpha$  is negative when the helicity of the forcing is positive, and  $\alpha$  changes sign when the helicity of the forcing changes sign. The magnitudes of  $\alpha$  are however different in the two cases:  $|\alpha|$  is larger when the helicity of the forcing is negative. In the sun, this corresponds to the sign of helicity in the northern hemisphere in the upper parts of the convection zone. This is here the relevant case, because the differential rotation pattern of the present model also corresponds to the northern hemisphere.

There is a striking difference between the cases with open and closed boundaries which becomes particularly clear when comparing the averaged values of  $\alpha$  for different magnetic Reynolds numbers; see Fig. 12. With closed boundaries  $\alpha$  tends to zero like  $R_m^{-1}$ , while with open boundaries  $\alpha$  shows no such decline. There is also a clear difference between the cases with and without shear together with open boundaries in both cases. In the absence of shear (dashed line in Fig. 12)  $\alpha$  declines with increasing  $R_m$ , even though for small values of  $R_m$  it is larger than with shear. The difference between open and closed boundaries will now be discussed in terms of a current helicity flux through the two open boundaries of the domain.

### 5.7 Current Helicity Flux

It is suggestive to interpret the above results in terms of the dynamical  $\alpha$  quenching model. However, (39) has to be generalized to take the divergence of the flux into account. In order to avoid problems with the gauge, it is advantageous to work directly with  $\overline{\mathbf{j} \cdot \mathbf{b}}$  instead of  $\overline{\mathbf{a} \cdot \mathbf{b}}$ . Using the evolution equation,  $\partial \mathbf{b} / \partial t = -\nabla \times \mathbf{e}$ , for the fluctuating magnetic field, where  $\mathbf{e} = \mathbf{E} - \overline{\mathbf{E}}$  is the small-scale electric field and  $\overline{\mathbf{E}} = \eta \mu_0 \overline{\mathbf{J}} - \overline{\mathcal{E}}$  the mean electric field, one can derive the equation

$$\frac{\partial}{\partial t} \overline{\mathbf{j} \cdot \mathbf{b}} = -2 \overline{\mathbf{e} \cdot \mathbf{c}} - \nabla \cdot \overline{\mathcal{F}_C^{\text{SS}}}, \quad (63)$$

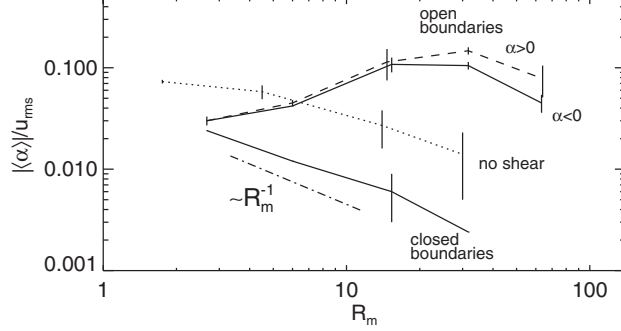


**Fig. 12.** Dependence of  $|\langle\alpha\rangle|/u_{\text{rms}}$  on  $R_m$  for open and closed boundaries. The case with open boundaries and negative helicity is shown as a dashed line. Note that for  $R_m \approx 30$  the  $\alpha$  effect is about 30 times smaller when the boundaries are closed. The *dotted line* gives the result with open boundaries but no shear. The *vertical lines* indicate the range obtained by calculating  $\alpha$  using only the first and second half of the time interval [Adapted from [Brandenburg and Subramanian \(2005\)](#)]

where

$$\overline{\mathcal{F}}_C^{\text{SS}} = \overline{2\mathbf{e} \times \mathbf{j}} + \overline{(\nabla \times \mathbf{e}) \times \mathbf{b}}/\mu_0, \quad (64)$$

is the current helicity flux from the small-scale field, and  $\mathbf{c} = \nabla \times \mathbf{j}$  the curl of the small-scale current density,  $\mathbf{j} = \mathbf{J} - \overline{\mathbf{J}}$ . In the isotropic case,  $\overline{\mathbf{e} \cdot \mathbf{c}} \approx k_f^2 \overline{\mathbf{e} \cdot \mathbf{b}}$ , where  $k_f$  is the typical wavenumber of the fluctuations, here assumed to be the forcing wavenumber. Ignoring the effect of the mean flow on  $\overline{\mathcal{E}}$  [as is usually done; but see [Krause and Rädler \(1980\)](#) and the recent on the shear current effect by [Rogachevskii and Kleeorin \(2003, 2004\)](#); see Sect. 4.5], we obtain

$$\overline{\mathbf{e} \cdot \mathbf{b}} \approx -\overline{(\mathbf{u} \times \mathbf{B}_0) \cdot \mathbf{b}} + \eta\mu_0 \overline{\mathbf{j} \cdot \mathbf{b}} = \overline{\mathcal{E} \cdot \mathbf{B}} + \eta\mu_0 \overline{\mathbf{j} \cdot \mathbf{b}}, \quad (65)$$

where we have used  $\overline{\mathbf{u} \times \mathbf{b}} = \overline{\mathcal{E}}$  and  $\mathbf{B}_0 = \overline{\mathbf{B}}$ . Using standard expressions for the turbulent magnetic diffusivity,  $\eta_t = \frac{1}{3}\tau u_{\text{rms}}^2$ , and the equipartition field strength,  $B_{\text{eq}} = \sqrt{\mu_0 \rho} u_{\text{rms}}$ , we eliminate  $\tau$  via

$$\frac{1}{3}\tau = \mu_0 \rho_0 \eta_t / B_{\text{eq}}^2. \quad (66)$$

This leads to an explicitly time dependent formula for  $\alpha$ ,

$$\frac{\partial \alpha}{\partial t} = -2\eta_t k_f^2 \left( \frac{\overline{\mathcal{E} \cdot \mathbf{B}} + \frac{1}{2}k_f^{-2} \nabla \cdot \mu_0 \overline{\mathcal{F}}_C^{\text{SS}}}{B_{\text{eq}}^2} + \frac{\alpha - \alpha_K}{R_m} \right). \quad (67)$$

This equation is similar to that of [Kleeorin et al. \(2000, 2002, 2003\)](#) who considered the flux of magnetic helicity instead of current helicity.

Making use of the adiabatic approximation, i.e. putting the rhs of (67) to zero, one arrives at the algebraic steady state quenching formula ( $\partial\alpha/\partial t = 0$ )

$$\alpha = \frac{\alpha_K + R_m \left( \eta_t \mu_0 \overline{\mathbf{J} \cdot \mathbf{B}} - \frac{1}{2}k_f^{-2} \nabla \cdot \mu_0 \overline{\mathcal{F}}_C^{\text{SS}} \right) / B_{\text{eq}}^2}{1 + R_m \overline{\mathbf{B}}^2 / B_{\text{eq}}^2}. \quad (68)$$

In the absence of a mean current, e.g. if the mean field is defined as an average over the whole box, then  $\overline{\mathbf{B}} \equiv \mathbf{B}_0 = \text{const}$ , and  $\overline{\mathbf{J}} = 0$ , so (68) reduces to

$$\alpha = \frac{\alpha_K - \frac{1}{2}k_f^{-2}R_m \nabla \cdot \mu_0 \overline{\mathcal{F}}_C^{\text{SS}} / B_{\text{eq}}^2}{1 + R_m \mathbf{B}_0^2 / B_{\text{eq}}^2}. \quad (69)$$

This expression applies to the present case, because we consider only the statistically steady state and we also define the mean field as a volume average.

For closed boundaries,  $\langle \nabla \cdot \overline{\mathcal{F}}_C^{\text{SS}} \rangle = 0$ , and so (69) clearly reduces to a catastrophic quenching formula, i.e.  $\alpha$  vanishes in the limit of large magnetic Reynolds numbers as

$$\alpha^{(\text{closed})} = \frac{\alpha_K}{1 + R_m \mathbf{B}_0^2 / B_{\text{eq}}^2} \rightarrow R_m^{-1} \quad (\text{for } R_m \rightarrow \infty). \quad (70)$$

The  $R_m^{-1}$  dependence is confirmed by the simulations (compare with the dash-dotted line in Fig. 12). On the other hand, for open boundaries the limit  $R_m \rightarrow \infty$  gives

$$\alpha^{(\text{open})} \rightarrow -(\nabla \cdot \mu_0 \overline{\mathcal{F}}_C^{\text{SS}}) / (2k_f^2 \mathbf{B}_0^2) \quad (\text{for } R_m \rightarrow \infty), \quad (71)$$

which shows that losses of negative helicity, as observed in the northern hemisphere of the sun, would enhance a positive  $\alpha$  effect (Kleeorin et al., 2000). In the simulations, the current helicity flux is found to be independent of the magnetic Reynolds number. This explains why the  $\alpha$  effect no longer shows the catastrophic  $R_m^{-1}$  dependence (see Fig. 12). In principle it is even conceivable that with  $\alpha_K = 0$  a current helicity flux can be generated, for example by shear, and that this flux divergence could drive a dynamo, as was suggested by Vishniac and Cho (2001). It is clear, however, that for finite values of  $R_m$  this would be a non-kinematic effect requiring the presence of an already finite field (at least of the order of  $B_{\text{eq}}/R_m^{1/2}$ ). This is because of the  $1 + R_m \mathbf{B}_0^2 / B_{\text{eq}}^2$  term in the denominator of (69). At the moment we cannot say whether this is perhaps the effect leading to the nonhelically forced turbulent dynamo discussed in Sect. 4.5, or whether it is perhaps the  $\boldsymbol{\delta} \times \overline{\mathbf{J}}$  or shear-current effect that was also mentioned in that section.

## 6 What about $\eta$ Quenching?

As we have seen above, in a closed domain the value of  $\alpha$  in the saturated state cannot conclusively be determined without also determining at the same time the turbulent magnetic diffusivity. There are different ways of determining  $\eta_t$ . The values are not necessarily all in agreement with each other, because one does not know whether the mean-field equation, where  $\eta_t$  enters, is correct and applicable. We report here a few different examples where  $\eta_t$  has been determined.

### 6.1 Direct Measurements in a Working Dynamo

We first consider the case of a helical turbulent dynamo without shear (B01) and compare it with a simple mean-field  $\alpha^2$  dynamo. Assuming that  $\alpha$  is uniform, we can use (31) and, assuming furthermore that  $\alpha < 0$  (which is the case when the helicity of the forcing is positive, as in B01), the solution is

$$\bar{\mathbf{B}} = (b_x \cos k_1 z, b_y \sin k_1 z, 0)^T. \quad (72)$$

The time-dependent equations can then be written as

$$\frac{db_x}{dt} = |\alpha|b_y - \eta_T k_1^2 b_x, \quad (73)$$

$$\frac{db_y}{dt} = |\alpha|b_x - \eta_T k_1^2 b_y. \quad (74)$$

In an isotropic, homogeneous  $\alpha^2$  dynamo, the eigenfunction obeys  $b_x = b_y$ .

We now assume that, at some particular time, we put  $b_x = 0$ , for example. This means that  $b_x(t)$  will first grow linearly in time at a rate that is proportional to  $\alpha$  like  $b_x \approx |\alpha|k_1 b_y$ . At the same time as  $b_x$  grows,  $b_y$  will first decrease at a rate that is proportional to  $\eta_T$ . This allows an independent estimate of  $b_x$  and  $b_y$  by solving the matrix equation

$$\begin{pmatrix} k_1 b_y & -k_1^2 b_x \\ k_1 b_x & -k_1^2 b_y \end{pmatrix} \begin{pmatrix} |\alpha| \\ \eta_T \end{pmatrix} = \begin{pmatrix} db_x/dt \\ db_y/dt \end{pmatrix}. \quad (75)$$

The result for  $\alpha$  is found to be roughly consistent with that of Cattaneo and Hughes (1996), and the result for  $\eta_T$  is reproduced in Fig. 13, and can be described by the fit formula

$$\eta_t = \frac{\eta_{t0}}{1 + \tilde{g}|\bar{\mathbf{B}}|/B_{\text{eq}}} \quad (76)$$

with  $\tilde{g} \approx 16$ . This expression needs to be compared with that obtained from other approaches.

The fact that the results obtained for  $\alpha$  by using this approach are consistent with that for a uniform field is quite surprising and unexpected. This agreement probably indicates that in this type of simulation  $\alpha$  is independent of scale – at least in the scale range corresponding to wavenumbers  $k = k_1 (= 1)$  and  $k = 0$ . In general, this may not be true. Indeed, in the case of accretion discs some numerical evidence for scale dependence of  $\alpha$  and  $\eta_t$  has been found (Brandenburg and Sokoloff, 2002).

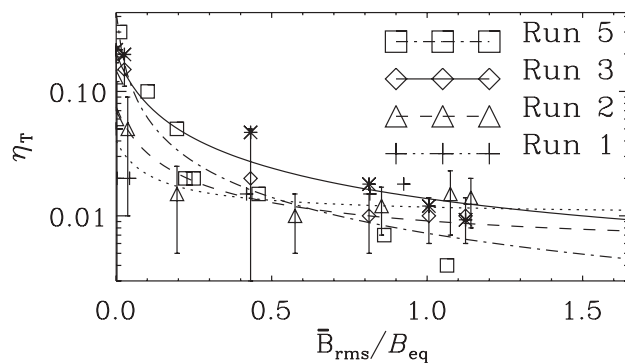


**Fig. 13.** Result for  $\eta_T$  for different values of  $R_m$ . The lines represent the fits described in the text. In the plot of  $\eta_T$  the asterisks denote  $|\alpha| - \lambda$  for the  $R_{m,\text{forc}} = 120$  run, which agrees reasonably well with  $\eta_T$  [Adapted from B01]

**Table 1.** Summary of the main properties of the three-dimensional simulations with shear. Here,  $\eta/(c_s k_1)$  is the magnetic diffusivity in units of the sounds speed and the wavenumber of the domain, and  $\omega_{\text{cyc}} = 2\pi/T_{\text{cyc}}$  is the cycle frequency. In Run (iii) there is no clear cycle visible [Adapted from BDS02]

Run	(i)	(ii)	(iii)
$\eta/(c_s k_1)$	$10^{-3}$	$5 \times 10^{-4}$	$2 \times 10^{-4}$
$\nu/\eta$	5	10	25
$R_m = \langle \mathbf{u}^2 \rangle^{1/2}/(\eta k_1)$	30	80	200
$C_\Omega = \langle \overline{\mathbf{U}}^2 \rangle^{1/2}/(\eta k_1)$	1000	2000	4000
$\langle \mathbf{b}^2 \rangle / B_{\text{eq}}^2$	4	6	20
$\langle \overline{\mathbf{B}}^2 \rangle / B_{\text{eq}}^2$	20	30	60
$\epsilon_m = \mu_0 \langle \overline{\mathbf{J}} \cdot \overline{\mathbf{B}} \rangle / \langle \overline{\mathbf{B}}^2 \rangle$	0.11	0.06	0.014
$\omega_{\text{cyc}}/(\eta k_1^2)$	8...9	6...12	$\geq 10?$

## 6.2 Measurements in an $\alpha\Omega$ Dynamo

In the case of an  $\alpha\Omega$  dynamo the cycle frequency  $\omega_{\text{cyc}}$  depends directly on the nonlinearly suppressed value of  $\eta_T$

$$\omega_{\text{cyc}} = \eta_T k_1^2 \quad (\eta_T \text{ is quenched}), \quad (77)$$

see BB02 (their Sect. 4.2). The estimates of BBS01 indicated that the dynamo numbers based on shear,  $C_\Omega = S/(\eta_T k_1^2)$ , is between 40 and 80, whilst the total dynamo number ( $\mathcal{D} = C_\alpha C_\Omega$ ) is between 10 and 20 (see BBS01), and hence  $C_\alpha = \alpha/(\eta_T k_1) \approx 0.25$ . Thus, shear dominates strongly over the  $\alpha$  effect ( $C_\Omega/C_\alpha$  is between 150 and 300), which is typical for  $\alpha\Omega$ -type behavior (i.e. oscillations) rather than  $\alpha^2$ -type behavior which would start when  $C_\Omega/C_\alpha$  is below about 10 (e.g. Roberts and Stix, 1972).

The results shown in Table 1 suggest that the period in this oscillatory dynamo is controlled by the microscopic magnetic diffusivity, because  $\omega_{\text{cyc}}/(\eta k_1^2)$  is approximately independent of  $R_m$ . Using (77), this means that  $\eta_T(\text{quenched})/\eta = \mathcal{O}(10)$  for  $R_m$  between 30 and 200. This result would favor a model where  $\eta_T$  is still quenched in an  $R_m$ -dependent fashion. In the next section we show that the apparent  $R_m$ -dependent  $\eta_t$  quenching can easily also be produced when the field possesses a helical component.

Looking at the scaling of the cycle frequency with resistivity may be quite misleading in the present case, because the large-scale magnetic field exceeds the kinetic energy by a large factor (20–30). This would always lead to the usual (non-catastrophic) quenching of  $\alpha$  and  $\eta_t$ . Furthermore, such strong magnetic fields will affect the mean shear flow. Most important is perhaps the fact that in the simulation of BBS01 the shear flow varies sinusoidally in the cross stream direction, so the mean field depends on the two coordinate directions perpendicular to the streamwise direction. For this reason BB02 solved the mean-field and dynamical quenching equations in a 2-dimensional model. It turned out to be important to allow for

**Table 2.** Results from the simulations of BBS01 and BDS02, compared with those of 2-dimensional mean-field models. Model results that are in fair agreement with the simulations are highlighted in bold face. Here,  $Q$  is the ratio of toroidal to poloidal rms field

Model	$R_m$	$C_\alpha$	$C_\Omega$	$\tilde{g}$	$\frac{S}{\eta k_1^2}$	$\frac{\langle \mathbf{b}^2 \rangle}{B_{\text{eq}}^2}$	$\frac{\langle \overline{\mathbf{B}}^2 \rangle}{B_{\text{eq}}^2}$	$Q^{-1}$	$\epsilon_m$	$\frac{\omega_{\text{cyc}}}{S}$	$\frac{\lambda}{\overline{S}}$
BBS01	80	1–2	–	–	2000	6	30	0.014	0.06	0.008	0.015
R1	20	1.0	100	0	2000	0.20	<b>15</b>	0.031	0.065	0.016	0.044
AG2	100	0.5	20	3	2000	0.10	<b>22</b>	0.011	0.024	<b>0.006</b>	<b>0.021</b>
BDS02	30	1–2	–	–	1000	4	20	0.018	0.11	0.014	0.006
s3	30	0.35	33	1	1000	0.07	6	0.029	<b>0.061</b>	<b>0.014</b>	<b>0.016</b>
S1	30	0.35	33	3	1000	0.07	<b>19</b>	0.009	0.019	0.005	0.016

non-catastrophic quenching of  $\eta_t$  using (76) where the value of  $\tilde{g}$  has been varied between 0 and 3. The asymptotic  $1/B$  behavior (as opposed to  $1/B^2$ , for example) was motivated both by simulations (B01) and analytic results (Kitchatinov et al., 1994; Rogachevskii and Kleeorin, 2001).

In order to see whether the models can be made to match the direct simulations, several input parameters were varied. It should be kept in mind, however, that not all input parameters are well known. This has to do with the uncertainty in the correspondence between the magnetic Reynolds number in the model (which measures  $\eta_{t0}/\eta$ ) and the simulations [where it is defined as  $u_{\text{rms}}/(\eta k_f)$ ]. Likewise, the dynamo number  $C_\alpha = \alpha/(\eta_T k_1)$  is not well determined. Nevertheless, many of the output parameters are reasonably well reproduced; see Table 2.

### 6.3 Decay Experiments

Finally, we consider the decay of a magnetic field. This provides a fairly straightforward method of determining  $\eta_T$  from the decay rate  $\lambda$  of a sinusoidal field with wavenumber  $k_1$ , so  $\lambda = \eta_T k_1^2$ . The result reported by Yousef et al. (2003) suggests that

$$\nu_t \approx \eta_t = (0.8 \dots 0.9) \times u_{\text{rms}}/k_f \quad (\text{for } \overline{\mathbf{B}}^2 \ll B_{\text{eq}}^2). \quad (78)$$

Once the mean flow profile has decreased below a certain level ( $< 0.1u_{\text{rms}}$ ), it cannot decay further and continues to fluctuate around  $0.08u_{\text{rms}}$ , corresponding to the level of the rms velocity of the (forced!) turbulence at  $k = k_1$  (see the dashed line in Fig. 14).

The quenching of the magnetic diffusivity,  $\eta_t = \eta_t(\overline{\mathbf{B}})$ , can be obtained from one and the same run by simply determining the decay rate,  $\lambda_B(\overline{\mathbf{B}})$ , at different times, corresponding to different values of  $\overline{\mathbf{B}} = |\overline{\mathbf{B}}|$ . To describe departures from purely exponential decay one can adopt a  $\overline{\mathbf{B}}$ -dependent  $\eta_t$  expression of the form (76). It turns out that the value of  $\tilde{g}$  is not universal and depends on the field geometry. This is easily demonstrated by comparing the decay of helical and nonhelical initial fields; see Fig. 15.

In the next section we show that the slower decay of  $\overline{\mathbf{B}}$ , and hence the implied stronger quenching of  $\eta_t$ , can also be described by a self-induced magnetic  $\alpha$  effect

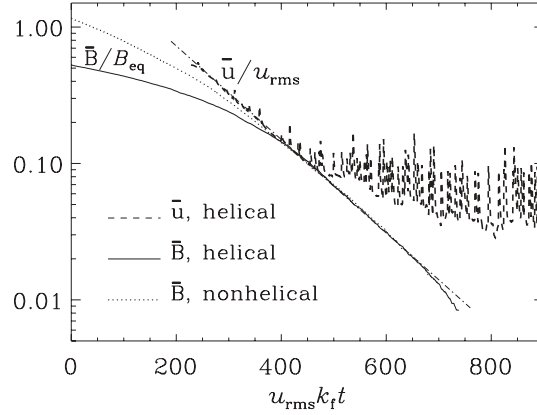


**Fig. 14.** Decay of large-scale helical velocity and magnetic fields (*dashed and solid lines*, respectively). The graph of  $\bar{U}(t)$  has been shifted so that both  $\bar{U}(t)$  and  $\bar{B}(t)$  share the same tangent (*dash-dotted line*), whose slope corresponds to  $\nu_t = \eta_t = 0.86 u_{rms}/k_f$ . The decay of a nonhelical magnetic field is shown for comparison (*dotted line*) [Adapted from Yousef et al. (2003)]

which acts such as to decrease the decay rate. In the case of a helical initial field, we have  $\bar{\mathbf{J}} \times \bar{\mathbf{B}} = 0$ , i.e. the large-scale field is force-free and interacts only weakly with the turbulence.

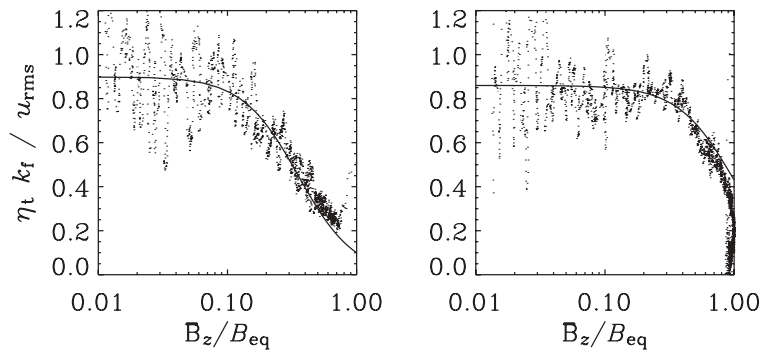


**Fig. 15.** Dependence of the turbulent diffusion coefficient on the magnitude of the mean field.  $R_m \approx 20$ . *Left:* The initial field is helical and corresponds to data points on the right hand side of the plot. The data are best fitted by  $\tilde{g} = 8 = 0.4 R_m$ . *Right:* the same for the nonhelical case. The data are best fitted by  $a = 1$ , independent of  $R_m$  [Adapted from Yousef et al. (2003)]

Thus, the indications here are that for non-helical fields,  $\eta_t$  is *not* catastrophically quenched. A resistively slow decay rate occurs however when the magnetic field is helical, but this is *not* to be explained by a catastrophically quenched  $\eta_t$ , but by

the magnetic  $\alpha$  effect,  $\alpha_M$ , that tries to keep the magnetic field as large as possible, just as enforced by the magnetic helicity constraint. The phenomenon, described in this way, may be more easily described in terms of helicity conservation, because the system has magnetic helicity that can only decay slowly on a resistive time scale, hence lowering the apparent turbulent diffusivity down to the microscopic value  $\eta$ . This will be explained in more detail in the next section.

#### 6.4 Taylor Relaxation or Selective Decay

In the case of a helical field with  $\overline{B}^2/B_{\text{eq}}^2 \gtrsim R_m^{-1}$  the slow decay of  $\overline{B}$  is related to the conservation of magnetic helicity. As already discussed by BB02, this behavior is related to the phenomenon of selective decay (e.g. Montgomery et al., 1978) and can be described by the dynamical quenching model. This model applies even to the case where the turbulence is nonhelical and where there is no  $\alpha$  effect in the usual sense. However, the magnetic contribution to  $\alpha$  is still non-vanishing, because it is driven by the helicity of the large-scale field.

To demonstrate this quantitatively, Yousef et al. (2003) have adopted the one-mode approximation ( $\mathbf{k} = \mathbf{k}_1$ ) with  $\overline{\mathbf{B}} = \hat{\mathbf{B}} \exp(i\mathbf{k}_1 z)$ , the mean-field induction equation

$$\frac{d\hat{\mathbf{B}}}{dt} = i\mathbf{k}_1 \times \hat{\mathcal{E}} - \eta k_1^2 \hat{\mathbf{B}}, \quad (79)$$

together with the dynamical  $\alpha$ -quenching formula (39),

$$\frac{d\alpha}{dt} = -2\eta k_f^2 \left( \alpha + \tilde{R}_m \frac{\text{Re}(\hat{\mathcal{E}}^* \cdot \hat{\mathbf{B}})}{B_{\text{eq}}^2} \right), \quad (80)$$

where

$$\hat{\mathcal{E}} = \alpha \hat{\mathbf{B}} - \eta_t i\mathbf{k}_1 \times \hat{\mathbf{B}} \quad (81)$$

is the electromotive force, and  $\tilde{R}_m$  is defined as the ratio  $\eta_{t0}/\eta$ , which is expected to be close to the value of  $R_m$ .

In Fig. 16 we show the evolution of  $\overline{B}/B_{\text{eq}}$  for helical and nonhelical initial conditions,  $\hat{\mathbf{B}} \propto (1, i, 0)$  and  $\hat{\mathbf{B}} \propto (1, 0, 0)$ , respectively. In the case of a nonhelical field, the decay rate is not quenched at all, but in the helical case quenching sets in for  $\overline{B}^2/B_{\text{eq}}^2 \gtrsim R_m^{-1}$ . In the helical case, the onset of quenching at  $\overline{B}^2/B_{\text{eq}}^2 \approx R_m^{-1}$  is well reproduced by the simulations. In the nonhelical case, however, some weaker form of quenching sets in when  $\overline{B}^2/B_{\text{eq}}^2 \approx 1$  (see the right hand panel of Fig. 15). We refer to this as standard quenching (e.g. (Kitchatinov et al., 1994) which is known to be always present; see (76)). BB02 found that, for a range of different values of  $R_m$ ,  $\tilde{g} = 3$  resulted in a good description of the simulations of cyclic  $\alpha\Omega$ -type dynamos (BDS02).

Yousef et al. (2003) also showed that the turbulent magnetic Prandtl number is indeed independent of the microscopic magnetic Prandtl number. The resulting values of the flow Reynolds number,  $\text{Re} = u_{\text{rms}}/(\nu k_f)$ , varied between 20 and 150, giving  $P_m$  in the range between 0.1 and 1. Within plot accuracy the three values of  $\lambda_B$  turn out to be identical in the interval where the decay is exponential.

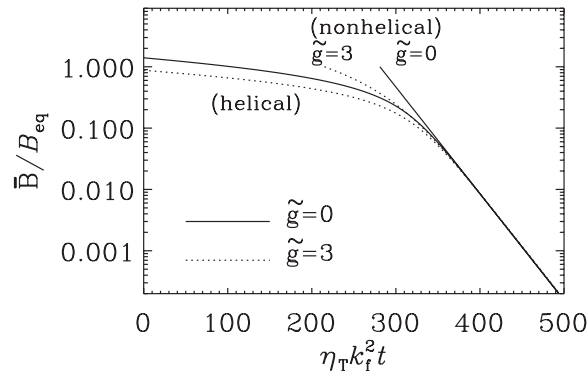


**Fig. 16.** Dynamical quenching model with helical and nonhelical initial fields. The quenching parameters are  $\tilde{g} = 0$  (solid line) and 3 (dotted line). The graph for the nonhelical cases has been shifted in  $t$  so that one sees that the decay rates are asymptotically equal at late times. The value of  $\eta_T$  used to normalize the abscissa is based on the unquenched value [Adapted from Yousef et al. (2003)]

## 7 Conclusions

In the present review we have tried to highlight some of the recent discoveries that have led to remarkable advances in the theory of mean-field dynamos. Of particular importance are the detailed confirmations of various aspects of mean-field theory using helically forced turbulence simulations. The case of homogeneous turbulence with closed or periodic boundary conditions is now fairly well understood. In all other cases, however, the flux of current helicity becomes important. The closure theory of these fluxes is still a matter of ongoing research (Kleeorin et al., 2000, 2002, 2003), Vishniac and Cho (2001), Subramanian and Brandenburg (2004), and Brandenburg and Subramanian (2005). The helicity flux of Vishniac and Cho (2001) has been independently confirmed (Subramanian and Brandenburg, 2004). A more detailed investigation of current helicity fluxes appears to be quite important when one tries to get qualitative and quantitative agreement between simulations and theory.

The presence of current helicity fluxes is particularly important when there is also shear. This was already recognized by Vishniac and Cho (2001) who applied their calculations to the case of accretion discs where shear is particularly strong. In the near future it should be possible to investigate the emergence of current helicity flux in more detail. This would be particularly interesting in view of the many observations of coronal mass ejections that are known to be associated with significant losses of magnetic helicity and hence also of current helicity ( DeVore, 2000; Démoulin et al., 2002; Gibson et al., 2002).

In order to be able to model coronal mass ejections it should be particularly important to relax the restrictions imposed by the vertical field conditions employed in the simulations of Brandenburg and Sandin (2004). A plausible way of doing this would be to include a simplified version of a corona with enhanced temperature and hence decreased density, making this region a low-beta plasma.

In the context of accretion discs the importance of adding a corona is well recognized (Miller and Stone, 2000), although its influence on large-scale dynamo action is still quite open. Regarding hydromagnetic turbulence in galaxies, most simulations to date do not address the question of dynamo action (Korpi et al., 1999; de Avillez and Mac Low, 2002).

This is simply because here the turbulence is driven by supernova explosions which leads to strong shocks. These in turn require large numerical diffusion, so the effective magnetic Reynolds number is probably fairly small and dynamo action may only be marginally possible. In nonhelically driven turbulence has been applied to the galactic medium to argue that it is dominated by small-scale fields (Schekochihin et al., 2002), but the relative importance of small-scale fields remains still an open question (Haugen et al., 2003). Galaxies are however rotating and vertically stratified, so the flows should be helical, but in order to say anything about magnetic helicity evolution, much larger magnetic Reynolds numbers are necessary. At the level of mean-field theory the importance of magnetic helicity fluxes is well recognized. The explicitly time-dependent dynamical  $\alpha$  quenching equation with magnetic helicity fluxes has been included in mean-field simulations (Kleeorin et al., 2000, 2002, 2003), but the form of the adopted fluxes is to be clarified in view of the differences with the results of Vishniac and Cho (2001) and Subramanian and Brandenburg (2004). Nevertheless, given that the form of the dynamical quenching equations is likely to be still incomplete, it remains to be demonstrated, using simulations, that magnetic or current helicity fluxes do really allow the dynamo to saturate on a dynamical time scale.

## Acknowledgements

The Danish Center for Scientific Computing is acknowledged for granting time on the Horseshoe cluster. This work has been completed while being on sabbatical at the Isaac Newton Institute for Mathematical Sciences in Cambridge.

## References

- de Avillez, M. A., Mac Low, M.-M.: 2002, ApJ 581, 1047 [251](#)  
 Balbus, S. A., Terquem, C.: 2001, ApJ 552, 235 [229](#)  
 Balsara, D., Pouquet, A.: 1999, Phys. Plasmas 6, 89 [240](#)  
 Beck, R., Brandenburg, A., Moss, D. et al.: 1996, ARA&A 34, 155 [220](#)  
 Berger, M., Field, G. B.: 1984, JFM 147, 133 [225](#)  
 Berger, M. A., Ruzmaikin, A.: 2000, JGR 105, 10481 [221](#), [235](#)  
 Boldyrev, S., Cattaneo, F.: 2004, Phys. Rev. Lett. 92, 144501 [221](#)  
 Blackman, E. G.: 2003, MNRAS 344, 707 [239](#)  
 Blackman, E. G., Field, G. F.: 2000, MNRAS 318, 724 [228](#)  
 Blackman, E. G., Field, G. B.: 2002, Phys. Rev. Lett. 89, 265007 [236](#)  
 Blackman, E. G., Brandenburg, A.: 2002, ApJ 579, 359 (BB02)  
 Blackman, E. G., Brandenburg, A.: 2003, ApJ 584, L99 [231](#)  
 Brandenburg, A.: 2001, ApJ 550, 824 (B01) [219](#)

- Brandenburg, A.: 2003, in *Simulations of Magnetohydrodynamic Turbulence in Astrophysics*, ed. E. Falgarone, T. Passot (Lecture Notes in Physics, Vol. 614. Berlin: Springer), p. 402 [220](#)
- Brandenburg, A., Dobler, W.: 2001, *A&A* 369, 329 [232](#)
- Brandenburg, A., Dobler, W.: 2002, *Comp. Phys. Comm.* 147, 471 [225](#)
- Brandenburg, A., Matthaeus, W. H.: 2004, *Phys. Rev. E* 69, 056407 [238](#), [239](#), [240](#), [242](#)
- Brandenburg, A., Sandin, C.: 2004, *A&A* 427, 13 [232](#), [233](#), [241](#), [250](#)
- Brandenburg, A., Sokoloff, D.: 2002, *Geophys. Astrophys. Fluid Dyn.* 96, 319
- Brandenburg, A., Subramanian, K.: 2005, *Phys. Rep.* [arXiv:astro-ph/0405052] [220](#), [222](#), [232](#), [235](#), [238](#), [243](#), [250](#)
- Brandenburg, A., Bigazzi, A., Subramanian, K.: 2001, *MNRAS* 325, 685 (BBS01) [229](#), [231](#)
- Brandenburg, A., Blackman, E. G., Sarson, G. R.: 2003, *Adv. Spa. Sci.* 32, 1835 [227](#), [232](#)
- Brandenburg, A., Dobler, W., Subramanian, K.: 2002, *AN* 323, 99 (BDS02) [228](#)
- Brandenburg, A., Nordlund, Å., Pulkkinen, P. et al.: 1990, *A&A* 232, 277 [241](#)
- Brun, A. S., Miesch, M. S., Toomre, J.: 2004, *ApJ* 614, 1073 [220](#)
- Cattaneo F., Hughes D. W.: 1996, *Phys. Rev. E* 54, R4532 [220](#), [237](#), [241](#)
- Chae, J.: 2000, *ApJ* 540, L115 [221](#), [235](#)
- Cowling, T. G.: 1934, *MNRAS* 94, 39 [219](#)
- Démoulin, P., Mandrini, C. H., van Driel-Gesztelyi, L. et al.: 2002, *Sol. Phys.* 207, 87 [250](#)
- DeVore, C. R.: 2000, *ApJ* 539, 944 [221](#), [235](#), [250](#)
- Field, G. B., Blackman, E. G.: 2002, *ApJ* 572, 685 [236](#)
- Gibson, S. E., Fletcher, L., Del Zanna, G. et al.: 2002, *ApJ* 574, 1021 [250](#)
- Gilman, P. A.: 1983, *ApJS* 53, 243 [220](#)
- Glatzmaier, G. A.: 1985, *ApJ* 291, 300 [220](#)
- Gruzinov, A. V., Diamond, P. H.: 1994, *Phys. Rev. Lett.* 72, 1651 [226](#), [237](#)
- Haugen, N. E. L., Brandenburg, A., Dobler, W.: 2003, *ApJ* 597, L141 [251](#)
- Haugen, N. E. L., Brandenburg, A., Dobler, W.: 2004, *Phys. Rev. E* 70, 016308 [221](#)
- Hollerbach, R., Rüdiger, G.: 2004, *MNRAS* 347, 1273 [230](#)
- Hughes D. W., Cattaneo F., Kim E. J.: 1996, *Phys. Lett.* 223, 167 [220](#)
- Kazantsev, A. P.: 1968, *Sov. Phys. JETP* 26, 1031 [220](#), [239](#)
- Keinigs, R. K.: 1983, *Phys. Fluids* 26, 2558 [238](#)
- Kitchatinov, L. L., Rüdiger, G., Pipin, V. V.: 1994, *AN* 315, 157 [247](#), [249](#)
- Kleeorin, N. I., Ruzmaikin, A. A.: 1982, *Magnetohydrodynamics* 18, 116 [237](#)
- Kleeorin, N. I., Moss, D., Rogachevskii, I., Sokoloff, D.: 2000, *A&A* 361, L5 [243](#), [244](#), [250](#), [251](#)
- Kleeorin, N. I., Moss, D., Rogachevskii, I., Sokoloff, D.: 2002, *A&A* 387, 453 [243](#), [250](#), [251](#)
- Kleeorin, N. I., Moss, D., Rogachevskii, I., Sokoloff, D.: 2003, *A&A* 400, 9 [243](#), [250](#), [251](#)
- Korpi, M. J., Brandenburg, A., Shukurov, A. et al.: 1999, *ApJ* 514, L99 [251](#)
- Krause, F., Rädler, K.-H.: 1980, *Mean-Field Magnetohydrodynamics and Dynamo Theory* (Berlin: Akademie-Verlag; also Oxford: Pergamon Press) [223](#), [226](#), [235](#), [243](#)
- Kulsrud, R. M., Anderson, S. W.: 1992, *ApJ* 396, 606 [226](#)
- Kulsrud, R. M.: 1999, *ARA&A* 37, 37 [220](#)
- Low, B. C.: 2001, *JGR* 106, 25,141 [221](#), [235](#)
- Maron, J., Blackman, E. G.: 2002, *ApJ* 566, L41 [228](#)
- Meneguzzi, M., Frisch, U., Pouquet, A.: 1981, *Phys. Rev. Lett.* 47, 1060 [240](#)
- Milano, L. J., Matthaeus, W. H., Dmitruk, P.: 2003, *Phys. Plasmas* 10, 2287 [240](#)
- Miller, K. A., Stone, J. M.: 2000, *ApJ* 534, 398 [251](#)
- Mininni, P. D., Gómez, D. O., Mahajan, S. M.: 2003, *ApJ* 587, 472 [230](#)
- Moffatt, H. K.: 1969, *JFM* 35, 117 [224](#)

- Moffatt, H. K.: 1978, *Magnetic Field Generation in Electrically Conducting Fluids* (Cambridge: Cambridge University Press) 223
- Montgomery, D., Turner, L., Vahala, G.: 1978, Phys. Fluids 21, 757
- Montgomery, D., Matthaeus, W. H., Milano, L. J., Dmitruk, P.: 2002, Phys. Plasmas 9, 1221 240
- Ossendrijver, M., Stix, M., Brandenburg, A.: 2001, A&A 376, 713 241
- Pouquet, A., Frisch, U., Léorat, J.: 1976, JFM 77, 321 236, 241
- Rädler, K.-H.: 1969, Geod. Geophys. Veröff., Reihe II 13, 131 235
- Roberts, P. H., Stix, M.: 1972, A&A 18, 453
- Rogachevskii, I., Kleorin, N.: 2001, Phys. Rev. E 64, 056307 247
- Rogachevskii, I., Kleorin, N.: 2003, Phys. Rev. E 68, 036301 220, 221, 235, 243
- Rogachevskii, I., Kleorin, N.: 2004, Phys. Rev. E 70, 046310 220, 221, 243
- Rogers, N. N., Denton, R. E., Drake, J. E. et al.: 2001, Phys. Rev. Lett. 87, 195004 230
- Rüdiger, G., Kitchatinov, L. L.: 1993, A&A 269, 581 241
- Schekochihin, A. A., Maron, J. L., Cowley, S. C., McWilliams, J. C.: 2002, ApJ 576, 806 251
- Schekochihin, A. A., Cowley, S. C., Maron, J. L., McWilliams, J. C.: 2004, Phys. Rev. Lett. 92, 054502 221
- Shukurov, A.: 2005, in *Mathematical Aspects of Natural Dynamos*, ed. E. Dormy (Dordrecht: Kluwer) (in press) [arXiv:astro-ph/0411739] 221
- Steenbeck, M., Krause, F.: 1969a, AN 291, 49 229
- Steenbeck, M., Krause, F.: 1969b, AN 291, 271 229
- Steenbeck, M., Krause, F., Rädler, K.-H.: 1966, Z. Naturforsch. 21a, 369 219
- Subramanian, K., Brandenburg, A.: 2004, Phys. Rev. Lett. 93, 205001 250, 251
- Vainshtein, S. I., Cattaneo, F.: 1992, ApJ 393, 165 226
- Vainshtein, S. I., Chitre, S. M., Olinto, A.: 2000, Phys. Rev. E 61, 44224430 230
- Vishniac, E. T., Brandenburg, A.: 1997, ApJ 475, 263 220
- Vishniac, E. T., Cho, J.: 2001, ApJ 550, 752 220, 221, 244, 250, 251
- Widrow, L. M.: 2002, Rev. Mod. Phys. 74, 775 220
- Yoshimura, H.: 1975, ApJS 29, 467 230
- Yousef, T. A., Brandenburg, A., Rüdiger, G.: 2003, A&A 411, 321 247, 248, 249, 250
- Zeldovich, Ya. B.: 1957, Sov. Phys. JETP 4, 460 219, 226